small amounts, they could not be classified according to size, as previously reported (Fig. 7B) [23,44,47]. In contrast, the majority of the wear particles from untreated CLPE surfaces were 0.1–1.0 μm across. In addition to enhancing the wear resistance of the cups, reducing bone resorptive responses to generated wear particles is important for preventing periprosthetic osteolysis. Such responses are dependent not only on the total amount of wear particles, but also on the proportion of particles that are within the most biologically active size range. The CLPE cups release a large number of sub-micrometer and nanometer-sized particles which are known to induce a greater inflammatory response than larger particles. Hence, although CLPE indeed causes a reduction in the total amount of particles, it might not necessarily lead to the prevention of periprosthetic osteolysis. Clinical evidence regarding the longevity of artificial joints with CLPE is anticipated in the future.

A previous study has shown that polymer particles covered with PMPC are biologically inert with respect to phagocytosis by macrophages and subsequent bone resorptive actions [48]. An increasing number of studies are exploring potential pharmacological modifications for the adverse host response to wear particles using agents such as cytokine antagonists, cyclooxygenase-2 inhibitors, and osteoprotegerin, or anti-RANKL (receptor activator of NF-κB ligand) antibody. However, they may cause serious side effects because the agents must be taken for a long period after surgery and because they are not currently targeted to the site of the problem. Surface modifications of MPC polymers for other medical devices have suppressed biologic reactions when they are in contact with living organisms [49] and are now clinically used on the surfaces of intravascular stents [50], soft contact lenses [51], and artificial lungs and hearts [52] under the authorization of the Food and Drug Administration of the United States. Hence, PMPC grafting is superior to these developing pharmacologic treatments, because the absence of side effects has already been confirmed clinically by several medical devices. In addition, based on other related evidences and multicenter clinical trials, the Japanese government (Ministry of Health, Labor, and Welfare) approved the clinical use of PMPC-grafted CLPE acetabular liners (Aquala® liner; Japan Medical Materials Corp.) in artificial hip joints in April 2011.

Despite these promising results, our study is subject to a number of limitations. First, we did not entirely capture the stabilities of the polyelectrolyte-grafted layers. Surface modification was accomplished using same photoinduced radical polymerization technique as that for methacrylate monomers. Hence, we believe the present surface modification layers combined with the substrate by strong C–C covalent bonding to attain similar stability. Second, we used a confined period for the hip simulator test. Although experiencing 3.0×10^6 cycles in the hip simulator is comparable to 3–5 years of physical walking, the duration may not be sufficiently long for young active patients. We are now running the hip simulator longer and thus far have confirmed almost no wear on the PMPC-grafted CLPE cups after 1×10^7 cycles [44]. Third, we did not entirely capture the range of loading and motion conditions of the *in vivo* environment in terms of the variety of positions, the magnitude of loading, or the daily routine, although we believe this, according to the ISO standard 14242-3, can provide some indication of the wear performances. Fourth, the procedure for the isolation of wear particles in this study does not entirely capture the contribution of wear particles with a diameter of less than 0.1 μm, as previously reported [53]. Cellular response to particles is thought to be dependent upon factors such as particle number, size, shape, surface area, and material chemistry. If nanometer-scaled particles are generated *in vivo*, it will be important to determine their biological activity in relation to that of micrometer-scaled particles. Fifth, the wear performance we report is only valid for this specific combination of Co–Cr–Mo alloy and polyelectrolyte-grafted CLPE. It was well known that protein molecules such as albumin from the lubricant are adsorbed more extensively on the surface of Co–Cr–Mo alloy than on other femoral component materials such as alumina, zirconia, and zirconia-toughened alumina [35–37,54]. Hence, we believe this study can provide more effective indication of the wear performance.

5. Conclusions

We evaluated the friction and wear performance of controlled, 100-nm-thick, uniform hydrophilic grafted polymer layers with various types of surface charge in various lubricant conditions and obtained clear preliminary evidence for their effectiveness. The primary mechanism underlying the low friction and high wear resistance must be attributed to the high level of hydration of the grafted layer, where water molecules act as very efficient lubricants. The secondary mechanism is considered to be repulsion of protein molecules and positively charged inorganic ions by the polyelectrolyte-grafted layer in a synovial fluid, which may reduce the adhesive interaction or interpenetration between opposing Co–Cr–Mo alloy surfaces themselves or between protein films adsorbed on the Co–Cr–Mo alloy. Finally, we showed that the nanometer-scaled hydrophilic polymer or polyelectrolyte layer on the CLPE surface can confer high durability to acetabular cup bearings in THA. Our findings may have implications on future studies on surface modification with cartilage-like or SPAL-like layers, which are of great importance in the design of lubricated surfaces for artificial joints.

Acknowledgments

This study was supported by Grants-in-Aid for Scientific Research (#23390359) from the Japanese Ministry of Education, Culture, Sports, Science and Technology, and by Health and Welfare Research Grants for Research on Medical Devices for Improving Impaired QOL (H20-004) and Research on Publicly Essential Drugs and Medical Devices (H23-007) from the Japanese Ministry of Health, Labour and Welfare. We thank Dr. Kozo Nakamura, National Rehabilitation Center for Persons with Disabilities, for the valuable discussions and suggestions.

References

[1] Kurtz S, Mowat F, Ong K, Chan N, Lau E, Halpern M. Prevalence of primary and revision total hip and knee arthroplasty in the United States from 1990 through 2002. J Bone Jt Surg Am 2005;87:1487–97.
[2] Harris WH. The problem is osteolysis. Clin Orthop Relat Res 1995;311:46–53.
[3] Sochart DH. Relationship of acetabular wear to osteolysis and loosening in total hip arthroplasty. Clin Orthop Relat Res 1999;363:135–50.
[4] Jacobs JJ, Roebuck KA, Archibeck M, Hallab NJ, Glant TT. Osteolysis: basic science. Clin Orthop Relat Res 2001;393:71–7.
[5] Glant TT, Jacobs JJ, Molnar G, Shanbhag AS, Valyon M, Galante JO. Bone resorption activity of particulate-stimulated macrophages. J Bone Miner Res 1993;8:1071–9.
[6] Kyomoto M, Iwasaki Y, Moro T, Konno T, Miyaji F, Kawaguchi H, et al. High lubricious surface of cobalt–chromium–molybdenum alloy prepared by grafting poly(2-methacryloyloxyethyl phosphorylcholine). Biomaterials 2007; 28:3121–30.
[7] Kyomoto M, Moro T, Iwasaki Y, Miyaji F, Kawaguchi H, Takatori Y, et al. Superlubricious surface mimicking articular cartilage by grafting poly(2-methacryloyloxyethyl phosphorylcholine) on orthopaedic metal bearings. J Biomed Mater Res A 2009;91:730–41.
[8] Kyomoto M, Moro T, Saiga K, Miyaji F, Kawaguchi H, Takatori Y, et al. Lubricity and stability of poly(2-methacryloyloxyethyl phosphorylcholine) polymer layer on Co–Cr–Mo surface for hemi-arthroplasty to prevent degeneration of articular cartilage. Biomaterials 2010;31:658–68.
[9] Kyomoto M, Ishihara K. Self-initiated surface graft polymerization of 2-methacryloyloxyethyl phosphorylcholine on poly(ether–ether–ketone) by photo-irradiation. ACS Appl Mater Interfaces 2009;1:537–42.

[10] Kyomoto M, Moro T, Takatori Y, Kawaguchi H, Nakamura K, Ishihara K. Novel self-initiated surface grafting with poly(2-methacryloyloxyethyl phosphorylcholine) on poly(ether–ether–ketone) biomaterials. Biomaterials 2010;31:1017–24.
[11] McMinn DJ, Daniel J, Pynsent PB, Pradhan C. Mini-incision resurfacing arthroplasty of hip through the posterior approach. Clin Orthop Relat Res 2005;441:91–8.
[12] Muratoglu OK, Bragdon CR, O'Connor DO, Jasty M, Harris WH. A novel method of cross-linking ultra-high-molecular-weight polyethylene to improve wear, reduce oxidation, and retain mechanical properties. Recipient of the 1999 HAP Paul Award. J Arthroplasty 2001;16:149–60.
[13] Chevalier J, Grandjean S, Kuntz M, Pezzotti G. On the kinetics and impact of tetragonal to monoclinic transformation in an alumina/zirconia composite for arthroplasty applications. Biomaterials 2009;30:5279–82.
[14] Kirk TB, Wilson AS, Stachowiak GW. The morphology and composition of the superficial zone of mammalian articular cartilage. J Orthop Rheumatol 1993;6:21–8.
[15] Bhosale AM, Richardson JB. Articular cartilage: structure, injuries and review of management. Br Med Bull 2008;87:77–95.
[16] Goldberg R, Schroeder A, Silbert G, Turjeman K, Barenholz Y, Klein J. Boundary lubricants with exceptionally low friction coefficients based on 2D close-packed phosphatidylcholine liposomes. Adv Mater 2011;23:3517–21.
[17] Goldberg R, Schroeder A, Barenholz Y, Klein J. Interactions between adsorbed hydrogenated soy phosphatidylcholine (HSPC) vesicles at physiologically high pressures and salt concentrations. Biophys J 2011;100:2403–11.
[18] Yamamoto M, Kato K, Ikada Y. Ultrastructure of the interface between cultured osteoblasts and surface-modified polymer substrates. J Biomed Mater Res 1997;37:29–36.
[19] Wang P, Tan KL, Kang ET. Surface modification of poly(tetrafluoroethylene) films via grafting of poly(ethylene glycol) for reduction in protein adsorption. J Biomater Sci Polym Ed 2000;11:169–86.
[20] Pavoor PV, Gearing BP, Muratoglu O, Cohen RE, Bellare A. Wear reduction of orthopaedic bearing surfaces using polyelectrolyte multilayer nanocoatings. Biomaterials 2006;27:1527–33.
[21] Kyomoto M, Moro T, Miyaji F, Hashimoto M, Kawaguchi H, Takatori Y, et al. Effects of mobility/immobility of surface modification by 2-methacryloyloxyethyl phosphorylcholine polymer on the durability of polyethylene for artificial joints. J Biomed Mater Res A 2009;90(2):362–71.
[22] Kyomoto M, Moro T, Konno T, Takadama H, Kawaguchi H, Takatori Y, et al. Effects of photo-induced graft polymerization of 2-methacryloyloxyethyl phosphorylcholine on physical properties of cross-linked polyethylene in artificial hip joints. J Mater Sci Mater Med 2007;18:1809–15.
[23] Kyomoto M, Moro T, Takatori Y, Kawaguchi H, Ishihara K. Cartilage-mimicking, high-density brush structure improves wear resistance of cross-linked polyethylene: a pilot study. Clin Orthop Relat Res 2011;469:2327–36.
[24] Raviv U, Klein J. Fluidity of bound hydration layers. Science 2002;297:1540–3.
[25] Ishihara K, Ueda T, Nakabayashi N. Preparation of phospholipid polymers and their properties as polymer hydrogel membranes. Polym J 1990;22(5):355–60.
[26] Xu ZK, Dai QW, Wu J, Huang XJ, Yang Q. Covalent attachment of phospholipid analogous polymers to modify a polymeric membrane surface: a novel approach. Langmuir 2004;20:1481–8.
[27] Kyomoto M, Moro T, Konno T, Takadama H, Yamawaki N, Kawaguchi H, et al. Enhanced wear resistance of modified cross-linked polyethylene by grafting with poly(2-methacryloyloxyethyl phosphorylcholine). J Biomed Mater Res A 2007;82(1):10–7.
[28] Kyomoto M, Moro T, Miyaji F, Hashimoto M, Kawaguchi H, Takatori Y, et al. Effect of 2-methacryloyloxyethyl phosphorylcholine concentration on photo-induced graft polymerization of polyethylene in reducing the wear of orthopaedic bearing surface. J Biomed Mater Res A 2008;86(2):439–47.
[29] Kyomoto M, Moro T, Miyaji F, Konno T, Hashimoto M, Kawaguchi H, et al. Enhanced wear resistance of orthopaedic bearing due to the cross-linking of poly(MPC) graft chains induced by gamma-ray irradiation. J Biomed Mater Res B Appl Biomater 2008;84:320–7.
[30] Kokubo T, Takadama H. How useful is SBF in predicting in vivo bone bioactivity? Biomaterials 2006;27:2907–15.
[31] Wright V, Dowson D. Lubrication and cartilage. J Anat 1976;121:107–18.
[32] Raviv U, Giasson S, Kampf N, Gohy JF, Jérôme R, Klein J. Lubrication by charged polymers. Nature 2003;425:163–5.
[33] Kobayashi M, Takahara A. Tribological properties of hydrophilic polymer brushes under wet conditions. Chem Rec 2010;10:208–16.
[34] Kobayashi M, Yamaguchi H, Terayama Y, Wang Z, Ishihara K, Hino M, et al. Structure and surface properties of high-density polyelectrolyte brushes at the interface of aqueous solution. Macromol Symp 2009;279:79–87.
[35] Serro AP, Gispert MP, Martins MC, Brogueira P, Colaço R, Saramago B. Adsorption of albumin on prosthetic materials: implication for tribological behavior. J Biomed Mater Res A 2006;78:581–9.
[36] Crockett R, Roba M, Naka M, Gasser B, Delfosse D, Frauchiger V, et al. Friction, lubrication, and polymer transfer between UHMWPE and CoCrMo hip-implant materials: a fluorescence microscopy study. J Biomed Mater Res A 2009;89:1011–8.
[37] Fang HW, Hsieh MC, Huang HT, Tsai CY, Chang MH. Conformational and adsorptive characteristics of albumin affect interfacial protein boundary lubrication: from experimental to molecular dynamics simulation approaches. Colloids Surf B Biointerfaces 2009;68:171–7.
[38] Kato K, Eika Y, Ikada Y. Deposition of a hydroxyapatite thin layer onto a polymer surface carrying grafted phosphate polymer chains. J Biomed Mater Res 1996;32:687–91.
[39] Tretinnikov ON, Kato K, Ikada Y. In vitro hydroxyapatite deposition onto a film surface-grated with organophosphate polymer. J Biomed Mater Res 1994;28:1365–73.
[40] Chen M, Briscoe WH, Armes SP, Klein J. Lubrication at physiological pressures by polyzwitterionic brushes. Science 2009;323:1698–701.
[41] Briscoe WH, Titmuss S, Tiberg F, Thomas RK, McGillivray DJ, Klein J. Boundary lubrication under water. Nature 2006;444:191–4.
[42] Kitano K, Inoue Y, Matsuno R, Takai M, Ishihara K. Nanoscale evaluation of lubricity on well-defined polymer brush surfaces using QCM-D and AFM. Colloids Surf B Biointerfaces 2009;74:350–7.
[43] Kobayashi M, Terayama Y, Hosaka N, Kaido M, Suzuki A, Yamada N, et al. Friction behavior of high-density poly(2-methacryloyloxyethyl phosphorylcholine) brush in aqueous media. Soft Matter 2007;2:740–6.
[44] Moro T, Takatori Y, Ishihara K, Nakamura K, Kawaguchi H. 2006 Frank Stinchfield Award: grafting of biocompatible polymer for longevity of artificial hip joints. Clin Orthop Relat Res 2006;453:58–63.
[45] Ishikawa Y, Hiratsuka K, Sasada T. Role of water in the lubrication of hydrogel. Wear 2006;261:500–4.
[46] Muratoglu OK, Wannomae K, Christensen S, Rubash HE, Harris WH. Ex vivo wear of conventional and cross-linked polyethylene acetabular liners. Clin Orthop Relat Res 2005;438:158–64.
[47] Moro T, Kawaguchi H, Ishihara K, Kyomoto M, Karita T, Ito H, et al. Wear resistance of artificial hip joints with poly(2-methacryloyloxyethyl phosphorylcholine) grafted polyethylene: comparisons with the effect of polyethylene cross-linking and ceramic femoral heads. Biomaterials 2009;30:2995–3001.
[48] Moro T, Takatori Y, Ishihara K, Konno T, Takigawa Y, Matsushita T, et al. Surface grafting of artificial joints with a biocompatible polymer for preventing periprosthetic osteolysis. Nat Mater 2004;3:829–37.
[49] Ueda H, Watanabe J, Konno T, Takai M, Saito A, Ishihara K. Asymmetrically functional surface properties on biocompatible phospholipid polymer membrane for bioartificial kidney. J Biomed Mater Res A 2006;77:19–27.
[50] Kuiper KK, Nordrehaug JE. Early mobilization after protamine reversal of heparin following implantation of phosphorylcholine-coated stents in totally occluded coronary arteries. Am J Cardiol 2000;85:698–702.
[51] Selan L, Palma S, Scoarughi GL, Papa R, Veeh R, Di Clemente D, et al. Phosphorylcholine impairs susceptibility to biofilm formation of hydrogel contact lenses. Am J Ophthalmol 2009;147:134–9.
[52] Snyder TA, Tsukui H, Kihara S, Akimoto T, Litwak KN, Kameneva MV, et al. Preclinical biocompatibility assessment of the EVAHEART ventricular assist device: coating comparison and platelet activation. J Biomed Mater Res A 2007;81:85–92.
[53] Tipper JL, Galvin AL, Williams S, McEwen HM, Stone MH, Ingham E, et al. Isolation and characterization of UHMWPE wear particles down to ten nanometers in size from in vitro hip and knee joint simulators. J Biomed Mater Res A 2006;78:473–80.
[54] Clarke IC, Green DD, Williams PA, Kubo K, Pezzotti G, Lombardi A, et al. Hip-simulator wear studies of an alumina-matrix composite (AMC) ceramic compared to retrieval studies of AMC balls with 1–7 years follow-up. Wear 2009;267:702–9.

PCCP

Dynamic Article Links

Cite this: *Phys. Chem. Chem. Phys.*, 2012, **14**, 10196–10206

www.rsc.org/pccp

PAPER

Mechanism underlying bioinertness of self-assembled monolayers of oligo(ethyleneglycol)-terminated alkanethiols on gold: protein adsorption, platelet adhesion, and surface forces†

Tomohiro Hayashi,*[ab] Yusaku Tanaka,[a] Yuki Koide,[a] Masaru Tanaka[c] and Masahiko Hara[ab]

Received 18th April 2012, Accepted 15th May 2012
DOI: 10.1039/c2cp41236e

The mechanism underlying the bioinertness of the self-assembled monolayers of oligo(ethylene glycol)-terminated alkanethiol (OEG-SAM) was investigated with protein adsorption experiments, platelet adhesion tests, and surface force measurements with an atomic force microscope (AFM). In this work, we performed systematic analysis with SAMs having various terminal groups (–OEG, –OH, –COOH, $–NH_2$, and $–CH_3$). The results of the protein adsorption experiment by the quartz crystal microbalance (QCM) method suggested that having one EG unit and the neutrality of total charges of the terminal groups are essential for protein-resistance. In particular, QCM with energy dissipation analyses indicated that proteins absorb onto the OEG-SAM *via* a very weak interaction compared with other SAMs. Contrary to the protein resistance, at least three EG units as well as the charge neutrality of the SAM are found to be required for anti-platelet adhesion. When the identical SAMs were formed on both AFM probe and substrate, our force measurements revealed that only the OEG-SAMs possessing more than two EG units showed strong repulsion in the range of 4 to 6 nm. In addition, we found that the SAMs with other terminal groups did not exhibit such repulsion. The repulsion between OEG-SAMs was always observed independent of solution conditions [NaCl concentration (between 0 and 1 M) and pH (between 3 and 11)] and was not observed in solution mixed with ethanol, which disrupts the three-dimensional network of the water molecules. We therefore concluded that the repulsion originated from structured interfacial water molecules. Considering the correlation between the above results, we propose that the layer of the structured interfacial water with a thickness of 2 to 3 nm (half of the range of the repulsion observed in the surface force measurements) plays an important role in deterring proteins and platelets from adsorption or adhesion.

Introduction

Nonfouling (anti-bioadhesion) surfaces have been widely demanded for various biomedical and biosensing applications, and many types of nonfouling surfaces have been reported so far. However, the mechanisms underlying nonfouling behavior have not been fully clarified at a molecular level.[1] In particular, self-assembled monolayers of oligo(ethyleneglycol)-terminated alkanethiol on gold (OEG-SAMs), which was first reported by Prime and Whitesides,[2,3] have provided a model system of protein- and cell-resistant surfaces. OEG-SAMs have been employed to suppress nonspecific adsorption of non-target molecules in biosensing and to pattern cells on solid substrates.[4,5] Although several models, which include electrostatic repulsion due to interfacial ions,[6] tightly bound water molecules,[7–9] and stable interfacial water layers,[10–13] have been proposed to explain the nonfouling behavior of OEG-SAMs, the question of why these monolayers, in which thiol molecules are densely packed compared with polymers grafted on surfaces, repel biomolecules and cells has remained unanswered.

The main problem in this field is that there has been little systematic work both on the interfacial behavior of water and

[a] *Department of Electronic Chemistry, Interdisciplinary Graduate School of Science and Engineering, Tokyo Institute of Technology, 4259 Nagatsuta-cho, Midori-ku, Yokohama, Kanagawa 226-8502, Japan. E-mail: hayashi@echem.titech.ac.jp*
[b] *Flucto-Order Functions Research Team, Advanced Science Institute, RIKEN, 2-1 Hirosawa, Wako, Saitama 351-0198, Japan*
[c] *Department of Biochemical Engineering, Graduate School of Science and Engineering, Yamagata University, Jonan 4-3-16, Yonezawa 992-0038, Japan*

† Electronic supplementary information (ESI) available: SEM images of self-assembled monolayers after the platelet adhesion experiments, interaction of the EG3–OH SAM (substrate) with NH_2–SAM (probe) in pure water, interaction of the EG3–OH SAM (substrate) with NH_2–SAM (probe) in solution at various pHs, and interaction of EG3–OH SAMs with the OH and C8 SAMs in pure water. See DOI: 10.1039/c2cp41236e

ions and on the results of protein adsorption and cell adhesion to clarify the mechanism underlying the bioinertness of OEG-SAMs. Among the few studies, Herrwerth *et al.* reported that the protein resistance of OEG-SAMs strongly depends on the density of the molecules constituting the SAM,[14] which was later supported by a report by Lee *et al.*[15] Moreover, Herrwerth *et al.* also stated that the internal hydrophilicity of the SAM (accommodation of water molecules in SAMs) and the hydrophilicity of the terminal groups (access of water molecules into SAMs) are key factors in protein resistance. Schilp *et al.* reported that the hydrophilicity of the terminal groups governs the resistance of the monolayer against the adhesion of algal cells.[7] Recently, the authors investigated the strength of the adhesion of fibroblast cells to OEG-SAMs and found a strong dependence of the strength of the adhesion on the number of EG units.[8]

Although the above reports clearly suggest that the manner of hydration (wetting) of the SAMs, which does not appear as a macroscopic wetting property, is a crucial factor for their protein resistance, details of the physical mechanism remain unclear with several questions arising: 1. What is the difference in wetting between protein adsorbing and protein resistant surfaces? 2. How thick is the interfacial water layer responsible for the protein resistance? 3. Are other interactions (*e.g.* electrostatic interaction) responsible for the protein resistance? To answer these questions, we require an understanding of the behavior of the interfacial water molecules and ions, which is speculated to play an important role in their bioinertness.

Surface force analyses mainly by atomic force microscopy (AFM)[16–18] and interfacial-force microscopy (IFM)[10] have been performed to investigate the behavior of interfacial ions or water molecules. Feldman *et al.* reported that the interaction between protein molecules (fibrinogen) and OEG-SAMs strongly depended on the density of the molecules constituting the SAM. In particular, they reported that protein-resistant Au-supported SAMs exhibited repulsion against the protein, with a clear correlation between the interaction and protein resistance. They concluded that the observed repulsion between the SAMs and proteins, which was considered to be responsible for the protein resistance, was due to electrostatic interaction. Later, Dicke and Hahner suggested that hydroxyl ions were immobilized at the interface between the SAM and bulk water and induced the electrostatic repulsion. On the other hand, Kim *et al.* reported that only water-induced repulsion was observed between the OEG-SAMs in pure water and that no electric double layer force was observed, contradicting the above reports.[10] The present situation clearly necessitates systematic analysis of the behavior of the interfacial ions and water with SAMs possessing various terminal groups.

In this work, we systematically investigated protein adsorption and platelet adhesion with SAMs having a variety of terminal groups including hydrophobic, polar, neutral, charged and different numbers of EG units (summarized in Table 1). Moreover, we investigated the interaction between the SAMs to elucidate the behavior of interfacial ions and water molecules. Based on the correlations among these results, we discuss the mechanism underlying the bioinertness of OEG-SAMs.

Experimental

Au(111) substrates and preparation of SAMs

Au(111) substrates were prepared by vacuum deposition of gold onto freshly cleaved mica ($10 \times 10 \times 0.3$ mm^3, S&J Trading Inc.) at 620 K under a vacuum pressure of 10^{-5}–10^{-6} Pa with a two-step evaporation process reported by Lüssem *et al.*[19] The substrates were then annealed at 620 K in a vacuum chamber for 2 h. The RMS roughness of the Au(111) substrate was about 0.3 nm. All thiol molecules were purchased from Sigma-Aldrich (St. Louis, USA) and ProChimia Surfaces (Gdańsk, Poland), and used without further purification. The monolayers of these thiol derivatives were formed by dipping the Au(111) substrates into freshly prepared ethanolic solutions containing the corresponding compounds at a concentration of 1 mM for 24 h. The chemical structures of the thiol molecules are summarized in Table 1. After the immersion, the samples were carefully rinsed with pure ethanol to remove physisorbed thiol molecules from the surface. The formation of SAMs (including the SAMs prepared on QCM sensors) according to the above approach was checked by X-ray photoelectron spectroscopy (XPS) measurements, which revealed the chemisorption of the sulfur head groups to the Au substrates.[20] The chemisorption of thiol molecules were confirmed also by thermal desorption spectroscopy.[21] The densities of the thiol molecules in the monolayers (shown in Table 1) were also evaluated by XPS (Supporting Information†).

PBS buffer

The phosphate buffered saline (PBS) buffer used in this work contains PBS (pH 7.4, 10 mM), containing NaCl (137 mM) and KCl (2.7 mM) (denoted as PBS). For the surface force analyses, the total concentration of NaCl was increased up to 0.6 M to investigate the effect of ion concentration on the interaction between the SAMs (denoted as PBS + NaCl in this article).

Water contact angle measurement

Static water contact angles were measured by the sessile-drop method on a Krüss DSA10 contact-angle meter. They were recorded at 25 ± 0.5 °C with distilled water. All droplets were 5 μL in volume.

QCM-D analysis

We employed a commercial QCM-D system (D300 Q-Sense, Sweden) to investigate the amount and viscoelastic properties of the proteins adsorbed on the SAMs.[22,23] First, Au-coated QCM sensors were cleaned by UV–ozone treatment. Then, the sensors were washed by sonication in the order of acetone, ethanol, and pure water, followed by drying with nitrogen. The SAMs were prepared with the same procedure as that for the Au(111) substrates. The proteins are human fibrinogen (Biogenesis, Poole, England) and BSA (Sigma-Aldrich, St. Louis, USA), which are major proteins in blood. The proteins were distributed as dried powder and carefully dissolved in PBS buffer. The results of dynamic light scattering (DLS) indicated that protein molecules are mono-dispersed, while maintaining their native shapes. In the QCM measurements, first, a measurement chamber was filled with PBS buffer; then protein dissolved in the PBS buffer at a

Table 1 A list of derivatives of alkanethiols used in this work

Abbreviation	Chemical structure of the thiol molecules	Static water contact angle (°)	Density with respect to alkanethiols
C8[a]	$HS–(CH_2)_7–CH_3$	112 (3.1)[c]	—
OH[a]	$HS–(CH_2)_{11}–OH$	17 (2.6)	98 (1.4)[d]
NH_2[b]	$HS–(CH_2)_{11}–NH_2$	35 (5.4)	97 (2.2)
COOH[b]	$HS–(CH_2)_{11}–COOH$	18 (4.4)	95 (2.0)
EG1–OH[b]	$HS–(CH_2)_{11}–(O–CH_2–CH_2)–OH$	33 (2.8)	94 (2.7)
EG2–OH[b]	$HS–(CH_2)_{11}–(O–CH_2–CH_2)_2–OH$	32 (3.5)	91 (2.3)
EG3–OH[b]	$HS–(CH_2)_{11}–(O–CH_2–CH_2)_3–OH$	32 (4.3)	86 (2.9)
EG3–OMe[b]	$HS–(CH_2)_{11}–(O–CH_2–CH_2)_3–O–CH_3$	69 (3.1)	88 (3.3)
EG3–NH_2[b]	$HS–(CH_2)_{11}–(O–CH_2–CH_2)_3–NH_2$	25 (5.2)	88 (3.5)
EG3–COOH[b]	$HS–(CH_2)_{11}–(O–CH_2–CH_2)_3–COOH$	22 (4.8)	89 (4.6)
EG6–OH[b]	$HS–(CH_2)_{11}–(O–CH_2–CH_2)_6–OH$	30 (4.2)	81 (4.4)

[a] Purchased from Sigma-Aldrich [b] Purchased from ProChimia Surfaces. [c] Numbers in parenthesis are standard deviations (n = 5). [d] Numbers in parenthesis are standard deviations (n = 12). The procedure for this analysis is explained in the Supporting information.

concentration of 1 mg ml^{-1} was injected. PBS buffer solution was injected again for rinsing, when the resonant frequency was stabilized. The changes in the resonant frequency (Δf) and energy dissipation (Δd) were defined as the differences in their values before the injection of the proteins and after the buffer solution rinse (Fig. 1). We calculated the amount of the adsorbed protein from the Sauerbrey equation:

$$\Delta m = -\frac{C \cdot \Delta f}{n}, \quad (1)$$

where C = 17.7 ng cm^{-2} Hz^{-1}, Δf is the change in the resonant frequency due to protein adsorption, and the n is the overtone number (n = 3 in this work). The dissipation factor D was measured by switching off the driving power and monitoring the amplitude decay profile. The amplitude decays as an exponentially damped sinusoidal function with a characteristic decay time (τ_0). The decay time is related to the dissipation factor (D) as follows:

$$D = \frac{1}{\pi f \tau_0} \quad (2)$$

$$D = \frac{1}{Q} = \frac{E_D}{2\pi E_S}, \quad (3)$$

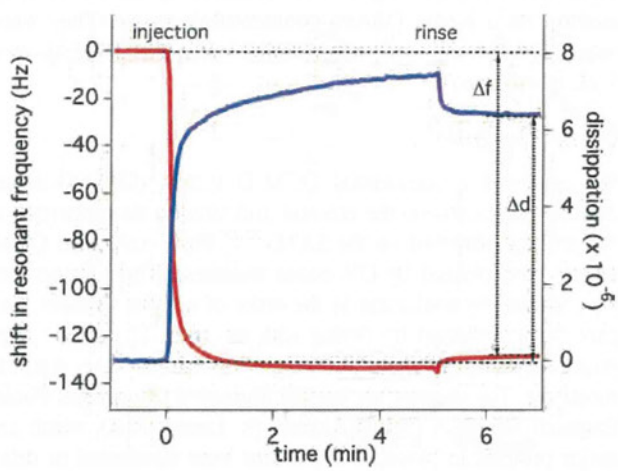

Fig. 1 Time course of the frequency and dissipation shifts for the adsorption of fibrinogen to the QCM sensor covered with the C8 SAM in the PBS solution. The changes in frequency (Δf) and dissipation (Δd) are defined as the difference between the values before the injection and after the rinsing as indicated by the arrows.

where f is the resonant frequency of the sensor, Q the quality factor, E_D the energy dissipated during one cycle, and E_s the energy stored in the oscillation. The volume and speed of buffer solution for rinsing were fixed throughout this work. The viscoelasticity of the protein layer was examined by comparing the values of Δd (change in energy dissipation)/Δf (change in resonant frequency) (Fig. 1). We performed three measurements for each system. One could expect that a rigid and compact layer would yield a small value of $\Delta d/\Delta f$.

Platelet adhesion test

Human blood was drawn from healthy volunteers and mixed with a 1/9 volume of acid citrate dextrose (ACD). Platelet-rich plasma (PRP) and platelet-poor plasma (PPP) were obtained by centrifugation of the blood at 1200 rpm for 5 min and at 3000 rpm for 10 min, respectively. Plasma containing 1×10^6 platelets mL^{-1} of platelet was prepared by mixing PRP with PPP. The platelet concentration was determined with a cell-counting hematocytometer (Neubauer chamber). Then, 200 μL of the plasma was placed on the SAMs, and incubated for 60 min at 37 °C. After the SAMs were washed three times with PBS buffer, they were immersed in 1% glutaraldehyde in PBS for 60 min at 37 °C to fix the adhered platelets. The SAMs were washed three times with PBS, washed with pure water and then immersed in ethanol to remove the water. The SAMs were sputter-coated with gold (thickness of approximately 2 nm) prior to observation with a scanning electron microscope (S-4800, HITACHI, Tokyo, Japan).

We prepared three substrates for each SAM, and acquired at least five images (30×40 μm^2) at different positions of each SAM. By counting the number of platelets in the image, the average densities of the platelets were calculated (n = 15).

Surface force analysis

All force curve measurements were performed with a commercial AFM system equipped with a liquid cell (MFP-3D, Asylum Research, Santa Barbara, CA). A silica bead (diameter 4 μm, Polysciences, Warrington, PA) was glued at the end of the tipless cantilever. The diameter of the bead was calibrated with its optical microscope image. Then, the probe was coated with Ti (thickness 2 nm, adhesion promoter) and Au (thickness 20 nm). The nominal spring constant of the cantilevers was 0.06 N m^{-1}. The spring constants were determined by monitoring the thermal

fluctuation of the levers. Probe velocity on approach was fixed at 200 nm s^{-1}. For the conversion of the deflection of the cantilever to the probe–surface separation, we simply defined a separation of zero as where linearity in the constant compliance region started in the force–displacement curve. The RMS roughnesses of the Au(111) substrate and Au-coated colloid probes were 0.3 and 0.6 nm, respectively. If we investigate the dependence of force on the solution conditions, we change solution with using the same sample in this work. In this work, the force is expressed based on the Derjaguin approximation (force/radius).

The high reproducibility of the force curves measured at different positions of the substrate was confirmed with the same system. As to the reproducibility of the force curves with different systems (substrate and cantilever) prepared with the same procedure, there are differences in the force/radius values up to 40%. We expect that the error originates mainly in uncertainty in the calibration of the spring constant of the cantilever by monitoring thermal noise and variations in the microscopic surface morphology of the colloid probes.

Results and discussion

Protein adsorption experiments

The results of the adsorption of fibrinogen and bovine serum albumin (BSA) onto the SAMs are summarized in Fig. 2. Our AFM imaging in liquid revealed that 75 to 90% of the surface area of the C8 SAM was covered with the protein molecules after exposure to the protein solution and rinsing. As is clearly seen, EG1–OH, EG2–OH, EG3–OH, EG3–OMe, and EG6–OH SAMs exhibited protein resistance, whereas the other SAMs adsorbed the proteins. This result suggests that at least one EG unit and the neutrality of charges of the terminal groups are necessary to deter the adsorption of proteins. Considering that the EG3–NH_2 and EG3–COOH SAMs adsorbed the proteins, charge neutrality was found to be a more important factor than the presence of the EG units for protein resistance.

Fig. 3 shows the relation between surface wettability (static water contact angle) and amount of adsorbed proteins. As is clearly seen, the affinity between protein and SAMs cannot be explained simply from macroscopic surface wettabilities. In particular, the EG3–OMe SAM exhibited protein resistance, despite its large contact angle compared with other hydrophilic SAMs. This result indicates that the protein resistance of OEG-SAMs cannot be explained by macroscopic surface wettabilities.

The relations between Δd and Δf provide deeper insight into the interaction between protein (fibrinogen) and SAMs (Fig. 4). The protein-resistant SAMs (red open symbols) showed higher $\Delta d/\Delta f$ values compared with other SAMs, whereas protein-adsorbing SAMs exhibited lower $\Delta d/\Delta f$ values. These differences in $\Delta d/\Delta f$ values originate in the differences in the viscoelasticity of the layer of adsorbed protein, which involves the interaction between the protein and SAM, the protein structures, and the structure of the water molecules hydrating the proteins, *etc*. Our results suggest that the proteins absorbed loosely to the hydrophilic SAM, whereas the protein molecules adsorbed onto the C8 SAM formed relatively rigid layers. Agnihotri and Siedlecki reported that the conformational change of fibrinogen adsorbed on hydrophobic surfaces is more significant than that on hydrophilic surfaces.[24] The formation of the rigid layer of fibrinogen on the C8 SAM is due to the strong hydrophobic interaction between the proteins and SAM, which may lead to denaturalization of the proteins and release of water molecules at the protein–SAM interface.

Compared to the case of C8 SAM, the proteins adsorbed on the protein-adsorbing hydrophilic SAMs formed a relatively soft layer. Most probably, the conformational change of the protein structure is not significant and the hydration shell of the protein is not largely disturbed, consistent with the previous findings obtained with AFM.[24–26] Comparing NH_2- and COOH-terminated SAMs, it was found that the EG3–NH_2 and EG3–COOH SAMs exhibited slightly larger $\Delta d/\Delta f$ values compared with those of the NH_2 and COOH SAMs, although the terminal groups are same. This result indicates that EG units tend to weaken the local SAM–protein interaction, while maintaining the native shape of the protein molecules.

Platelet adhesion tests

The densities of the platelets on the SAMs are summarized in Fig. 5. Anti-platelet adhesion was confirmed for EG3–OH, EG3–OMe, and EG6–OH SAMs but not for the other SAMs. Similar to the results of the protein adsorption experiment, in

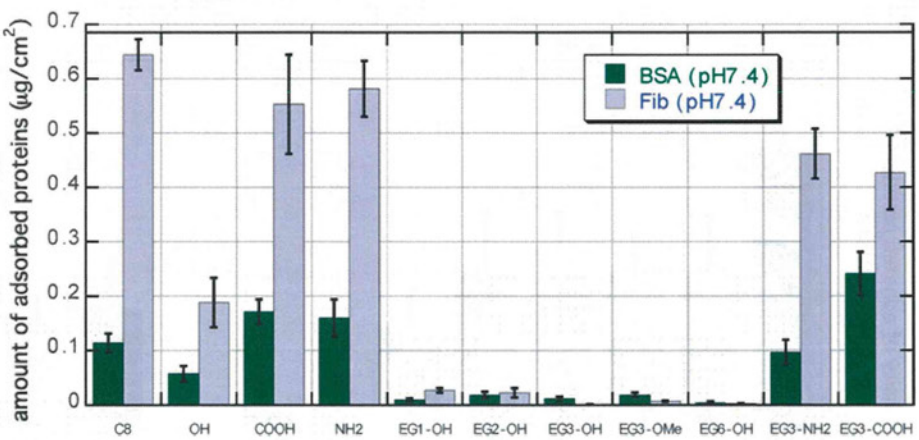

Fig. 2 The amounts of adsorbed BSA and fibrinogen in the PBS solution measured by QCM. The amount is defined in Fig. 1 and its caption. Error bars denote standard deviation (n = 4).

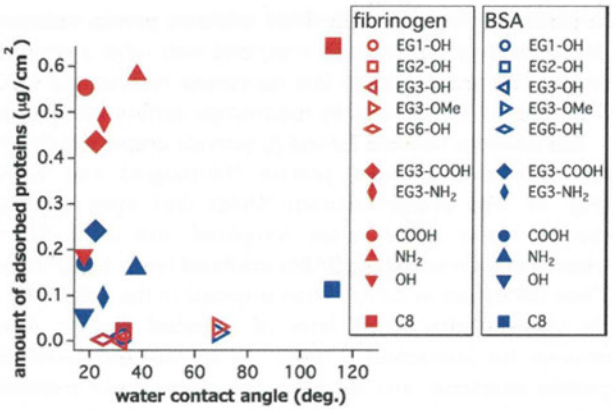

Fig. 3 The amounts of adsorbed BSA and fibrinogen in the PBS solution (same data presented in Fig. 2), plotted as a function of water contact angles.

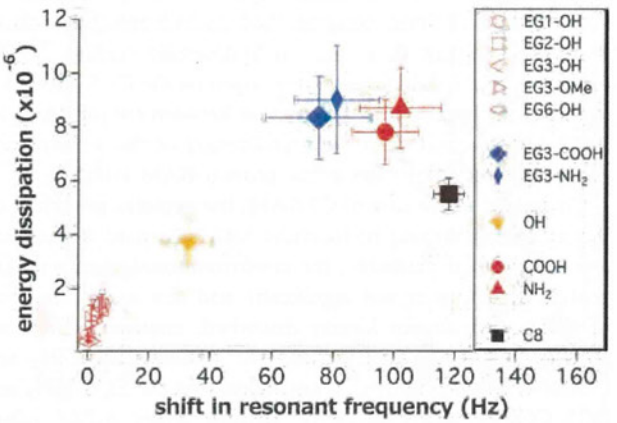

Fig. 4 The changes in dissipation (Δd) plotted against the frequency shifts (Δf) in the case of fibrinogen.

the cases of the OEG-SAMs, the neutrality of the total charge of the terminal groups is essential for anti-platelet adhesion. The relation between the density of the adhered platelets and the water contact angles of the SAMs is plotted in Fig. 6. The results for the anti-platelet-adhesion SAMs were completely off from the density–wettability relation for the other SAMs, indicating that the resistance to platelet adhesion cannot be explained by macroscopic surface wettabilities, as is the case with protein resistance.

We next discuss the degree of the activation of the platelets on the SAMs. The adhered platelets were simply classified into three types: *i.e.*, (a) native (round shape) and (b) partially activated (showing protruding pseudopodia), and (c) completely denatured (flat shape) (Fig. 7). The results of the classification are summarized in Table 2. The degree of the activation was prominent for the C8 SAM compared with the other SAMs. Among the other SAMs, the EG1–OH and EG2–OH SAMs induced much less activation of the adhered platelets (22 and 15%, respectively).

In general, when a surface is exposed to blood, the surface is hydrated, immediately followed by the adsorption of proteins. After that, platelets adhere to the adsorbed proteins, using them as an extracellular matrix. Among the proteins, fibrinogen has been considered as a major determinant for the response (adhesion and activation) of platelets. In particular, Tanaka *et al.* and Sivaraman and Latour recently reported that the conformation of adsorbed fibrinogen (content of α-helix) affects the activation of the platelets rather than the amount of the adsorbed fibrinogen.[27,28] Considering the SAMs without an EG unit, the activation of the platelets [sum of percentages of type (b) and (c)] are significant in the order of the series of C8, NH_2, COOH, and OH. This tendency is consistent with the order of $\Delta d/\Delta f$ values [C8, NH_2 and COOH (almost equal to NH_2), and OH]. As for the OEG-SAMs, the activation of the platelets is significantly lower and their $\Delta d/\Delta f$ values are high compared with those of other SAMs. These results confirm the conclusions of Tanaka *et al.* and Sivaraman and Latour.[27,28]

Comparing the degree of platelet activation for EG3–COOH and EG3–NH_2 with those for NH_2 and COOH, some effects of the EG unit on the conformation of the adsorbed fibrinogen and the activation of the platelets obviously exist. Another interesting issue is that EG1–OH and EG2–OH SAMs adhered platelets, whereas the EG3–OH, EG3–OMe and EG6–OH SAMs deterred platelets from adhesion, clearly displaying the effect of the number of the EG units on the response of platelets after the adhesion. This result suggests the strong dependence of the behavior of the interfacial water molecules or ions on the number of EG units.

Surface force measurements

Fig. 8(a) shows force–separation curves for approaching EG3–OH SAMs facing each other in pure water and PBS solution.

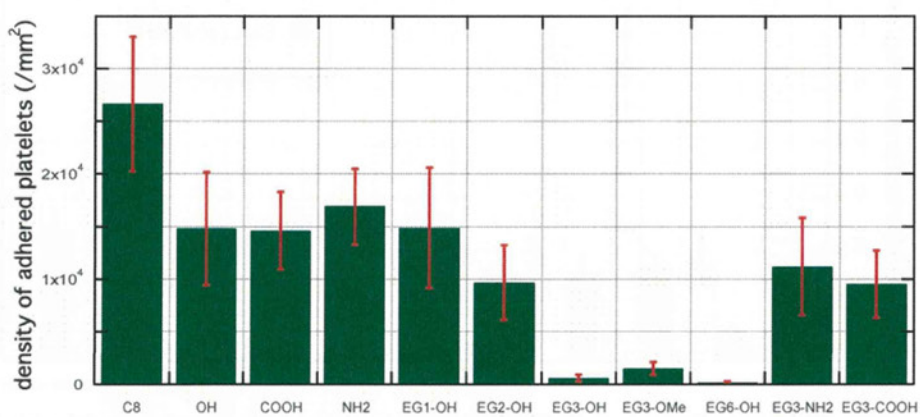

Fig. 5 Density of the adhered platelets on the SAMs. Error bars denote standard deviation (n = 15).

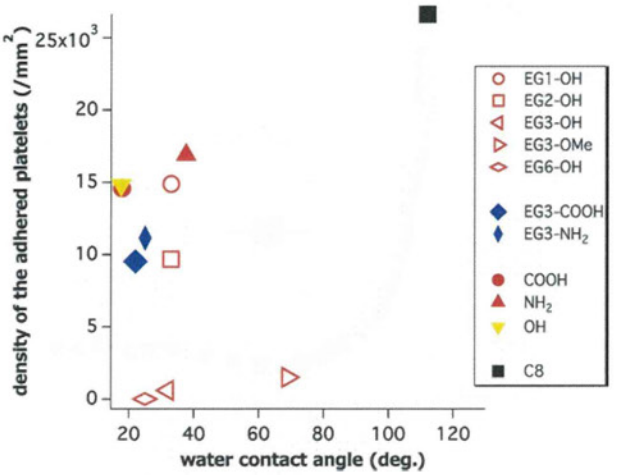

Fig. 6 Density of the adhered platelets on the SAMs (same data presented in Fig. 5) plotted as a function of water contact angles.

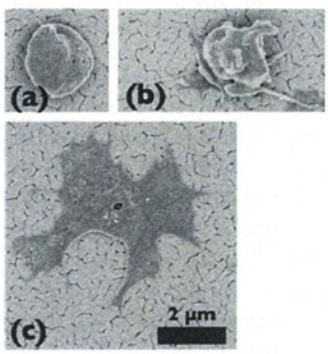

Fig. 7 SEM images of three typical shapes of the adhered platelets (measured with the OH-SAM): (a) native (round shape), (b) partially denatured (pseudopodia present), and (c) fully denatured (flattened).

Table 2 Percentages of native, partially and fully denatured platelets on each SAM

SAM	Native shape	Partially denatured	Fully denatured
C8	0 (0)	26 (5.2)	74 (11)
OH	54 (13)	34 (8.1)	12 (2.6)
NH_2	26 (6.0)	46 (9.2)	28 (5.4)
COOH	38 (7.3)	35 (7.9)	27 (4.4)
EG1–OH	78 (19)	18 (5.2)	4 (2.8)
EG2–OH	85 (16)	13 (2)	2 (0.62)
EG3–OH	97 (4.2)	3 (0.23)	0
EG3–OMe	99 (2.2)	1 (0.08)	0
EG3–NH_2	81 (13)	14 (4.3)	5 (1.2)
EG3–COOH	79 (16)	17 (3.2)	4 (1.5)
EG6–OH	100 (0)	0 (0)	0 (0)

Numbers in parenthesis are standard deviations (n = 15).

In pure water, a long-range repulsion was observed, whereas the repulsion disappeared in the PBS and PBS + NaCl solutions. Therefore, we concluded that the repulsion originated from electrostatic interaction. To estimate the surface charge density of the SAMs, we performed a fitting of the curve based on the Derjaguin, Landau, Verwey and Overbeek (DLVO) theory (Fig. 8(b)).[29] In the case of interaction between a sphere with a diameter of R and a flat surface, the electrostatic double-layer force interacting between them at a larger separation (> 10 nm),

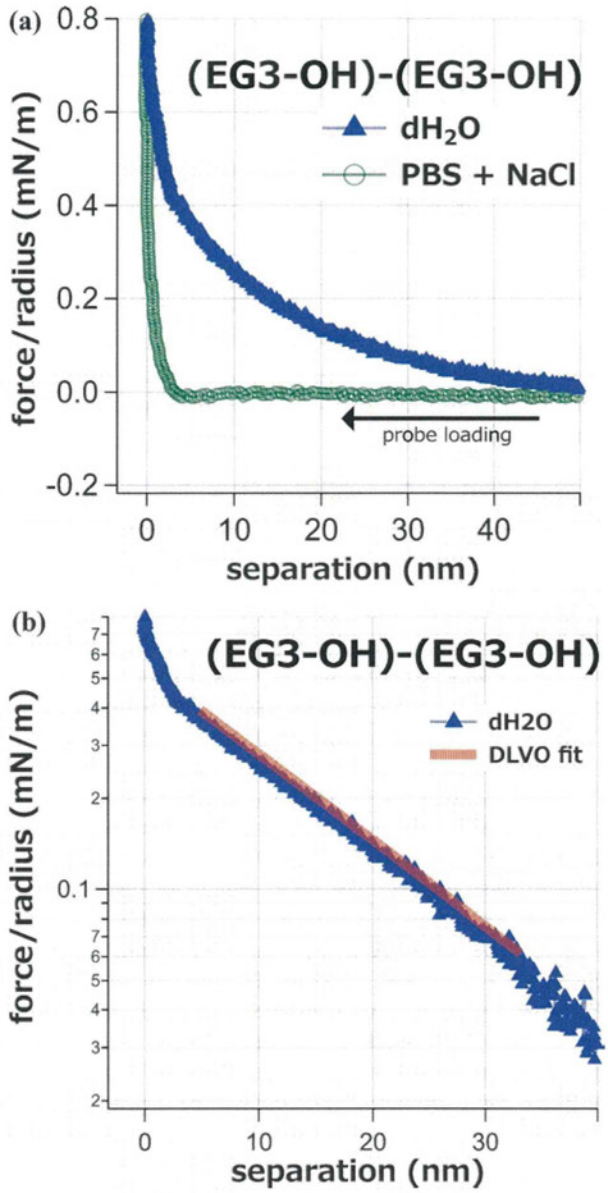

Fig. 8 (a) Force–separation curves recorded on the approach of a probe (EG3–OH) to the substrate (EG3–OH) in pure water and PBS + NaCl solution. (b) The force–distance curve obtained in pure water plotted on a semi-logarithmic scale and the results of the fitting to DLVO theory.

where the surfaces charges are considered constant, can be expressed as:

$$F_{\text{electrostatic}}(D) = \frac{4\pi R\sigma_S\sigma_T\lambda_D}{\varepsilon_0}\exp^{-D/\lambda_D} \qquad (4)$$

where D is the separation between the probe and surface, λ_D is the Debye decay length and σ_S and σ_T are the net charge densities of the surface and probe (these were assumed to be identical in the fittings).[30] σ was estimated to be 0.006 electron per nm^2 (corresponding to about 13 × 13 nm^2 per charge). We next discuss the interaction between the EG3–OH and NH_2 SAMs. We observed the long-range attraction between them in pure water (supporting information†). As the zeta potential of the NH_2 SAM in pure water is positive, the negative ions

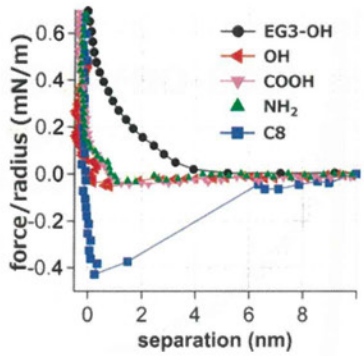

Fig. 9 Force–separation curves recorded on an approach for symmetric systems of the SAMs (the same SAMs prepared for both the probe and substrate) in PBS + NaCl solution.

are considered to be concentrated in the vicinity of the EG3–OH SAM. Combining this finding with those of previous reports, we concluded that hydroxyl ions are the origin of the negative charge.

Fig. 9 displays the force–distance curves measured with the SAMs with various terminal groups in the PBS + NaCl solution. In these experiments, the same SAMs were prepared on both the probe and the substrate. The hydrophobic C8 SAMs showed attraction (jump-in) from a distance of about 6 nm. This attraction is most probably attributed to van der Waals and hydrophobic interactions. In the cases of the hydrophilic OH SAM, only weak attraction was observed. As to the charged hydrophilic NH_2 and COOH SAMs, very short-range repulsion was observed. The decay lengths of these repulsions (0.36 nm) were close to the Debye length of the PBS + NaCl solution (0.38 nm). Although the electrostatic interaction between the EG3–OH SAMs disappeared in PBS and PBS + NaCl solution, it was confirmed that repulsion still existed even in PBS + NaCl solution. The decay length of the repulsion was 1.4–1.6 nm, which is much larger than the Debye length of the PBS + NaCl solution. We examined the dependence of the repulsion on the concentration of NaCl in solution, and found that the decay lengths of the repulsion were far beyond the Debye lengths of the solutions (supporting information†). Therefore, another interaction besides the DLVO force must have contributed to the repulsion between the EG3–OH SAMs.

We measured the interaction between the EG3–OH SAMs in solution at a pH of 4.3, where we found that the electrostatic repulsion was minimized (an isoelectric point of the SAM) (Fig. 10).

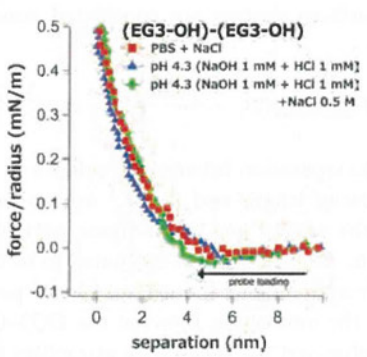

Fig. 10 Interaction between the EG3–OH SAMs in solution at pH 4.3 (isoelectric point of the EG3–OH SAM) with different ion concentrations.

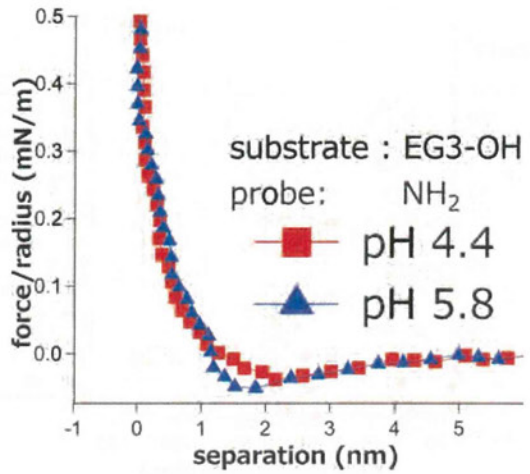

Fig. 11 Force–separation curves recorded on the approach of the NH_2 SAM (probe) to EG3–OH SAMs (substrate) in solutions with different pH values (4.4 and 5.8). The pH values were adjusted by mixing HCl (1 mM) and NaOH (1 mM). The results obtained with other pH values are presented in the Supporting Information.†

The interaction measured at pH 4.3 (NaOH 1 mM + HCl 1 mM) is very similar to that obtained in the other pH 4.3 solution to which NaCl was added (0.5 M) and to that obtained in the PBS + NaCl solution. Under these solution conditions, the electrostatic DLVO force was minimized. We did not observe long-range electrostatic repulsion, and only a repulsion arising from a separation of 6 nm was confirmed. In addition, we observed the repulsion for all solution conditions (pH and ion concentration), strongly indicating that the repulsion has no electrostatic character.

Next, we discuss the interaction of the EG3–OH SAM with the NH_2 SAM, whose isoelectric point differs from that of the EG3–OH SAM (Fig. 11). The interaction strongly depended on the pH value of the solution (supporting information†), and attraction was observed at pH 4.4 and 5.8. In these conditions, the zeta potentials of the EG3–OH and NH_2 SAMs are considered negative and positive, respectively, resulting in attractive electrostatic interaction. Even in such a situation, the repulsion was observed at a separation smaller than 1.5 nm. It is easily concluded that the repulsion cannot be originated from electrostatic interaction. It should also be noted that the operating length of the repulsion in this case was about half that observed between the EG3–OH SAMs.

Fig. 12 shows the interaction of the EG3–OH SAM with other SAMs with various surface wettabilities (EG3–OH, OH, and C8 SAMs). In pure water, electrostatic long-range repulsion was observed in all three cases (supporting information†). In the PBS + NaCl solution, the long-range DLVO force disappeared and short-range repulsion remained. The short-range repulsion was the strongest against EG3–OH and was the weakest against the C8 SAM. (Note that similar results were also reported by Kim *et al.*,[10] however, they observed these interactions in deionized water). As shown in Fig. 9, the repulsion attributed to the deformation of the monolayers was not observed for the C8 and OH SAMs. Therefore, the difference in the molecular length (thickness of the monolayer) is not the cause of differences in the range of repulsion among these systems. These results imply that water molecules in the vicinity of the EG3–OH SAM

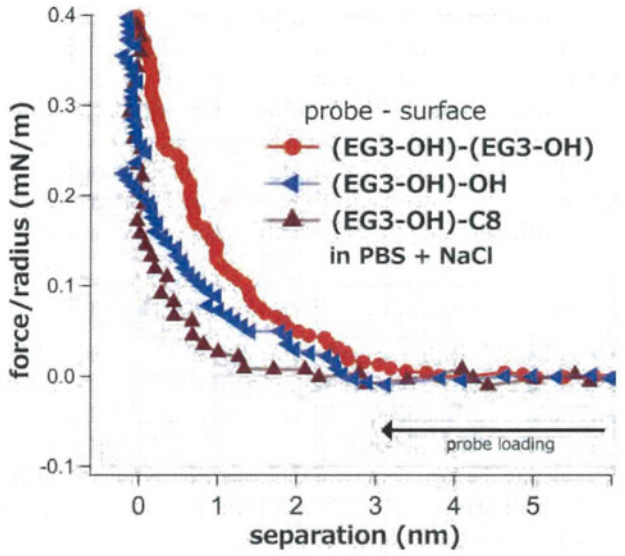

Fig. 12 Force *vs.* distance curves recorded on the approach of the EG3–OH SAM (probe) to various neutral SAMs (substrate) with different water wettabilities in PBS + NaCl solution. Through this experiment, the same probe was used and only the substrates were changed.

are involved in the repulsion, since the wettability of the opposing surface may affect the structure and dynamics of water in the confined region.

To investigate the dependence of the interaction on the number of EG units, we measured the interaction between the EG1–OH, EG2–OH, EG3–OH, EG3–OMe, and EG6–OH SAMs. As presented in Fig. 13(a), long-range DLVO repulsion with a decay length ranging between 20 and 30 nm was observed for all these SAMs. Our measurements of interactions of these SAMs with the NH_2 SAM revealed that these SAMs are negatively charged (most probably due to hydroxide ions). On the other hand, there are noticeable differences in the short-range interaction observed at separations smaller than 10 nm. In the cases of EG1–OH and EG2–OH, the contribution of repulsive force to the total interaction is clearly small compared with the cases of EG3–OH, EG3–OMe, and EG6–OH.

In PBS + NaCl solution, the differences in the short-range repulsions are obvious (Fig. 13(b)). That is, the repulsive interaction is dominant for EG3–OH, EG3–OMe, and EG6–OH, whereas the interaction observed for the EG1–OH and EG2–OH SAMs was dominated by attraction at any separation. The above difference cannot be explained by the differences in hydrophobic and van der Waals interactions. The deformation of the films, especially the EG moieties, after their mechanical contact is also ruled out from the origin of the repulsion, since the difference in the molecular length of EG1–OH and EG3–OH is estimated to be about 0.8 nm, which is much shorter than the range of the repulsion.

We next performed the force–distance curve measurements in a mixture of water (buffer) and ethanol to verify the possibility of water-mediated force. It is well-known that ethanol alters the hydrogen bond networks of water molecules. The force–separation curves in Fig. 14(a) were measured in mixtures of water and ethanol at different mixing ratios. Long-range repulsion, which had been considered a DLVO force, was observed at any molar fraction of ethanol (P_{et}),

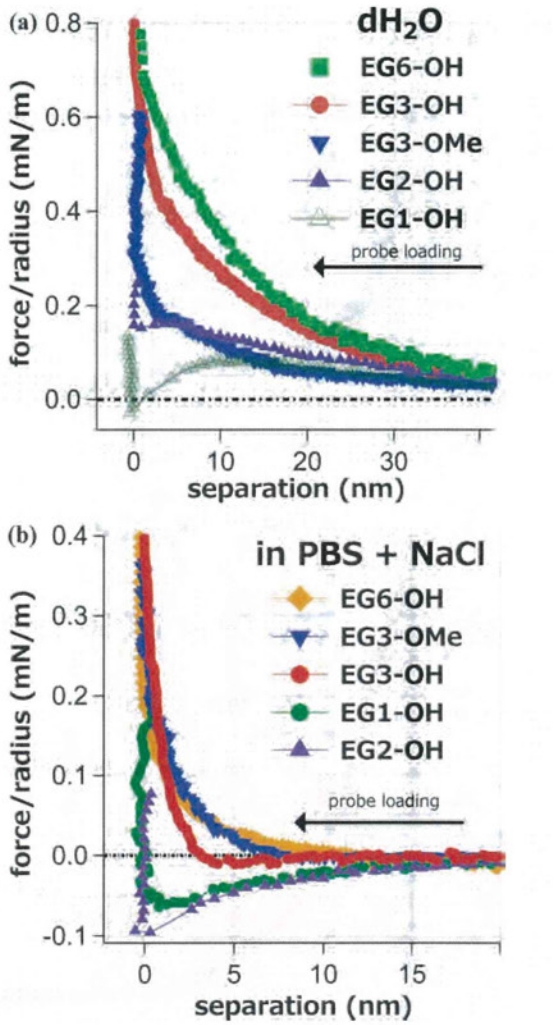

Fig. 13 Comparison of the approaching force curves for symmetric systems of the OEG-SAMs measured in (a) pure water and (b) PBS + NaCl solution.

indicating that ethanol does not affect the behavior of the interfacial hydroxide ions. By contrast, short-range repulsion was not observed, when P_{et} was above 0.17. In the mixture of the PBS + NaCl solution and ethanol, we did not observe repulsion at a P_{et} of 0.23 (Fig. 14(b)). Based on these results, we concluded that ethanol significantly affects the short-range repulsion. We here considered the effect of the conformational change in the EG chain. The difference in the thicknesses of the EG3–OH SAMs in all-*trans* and helical conformations is estimated to be 0.2 nm. Therefore, the conformational change in the EG part cannot be the reason for the absence of repulsion in the water–ethanol mixtures. The disappearance of the repulsion was not explained by the difference in the van der Waals interaction, since the Hamaker constants of the PBS buffer (3.7×10^{-20} J) and the mixture of PBS + NaCl and ethanol (3.8×10^{-20} J) preclude a significant effect on the van der Waals interaction.

Previous studies of the structure of water–ethanol solutions have indicated that microscopic phase separation between water and ethanol occurs at P_{et} values lower than 0.08 and that complete mixing and disruption of the hydrogen bond

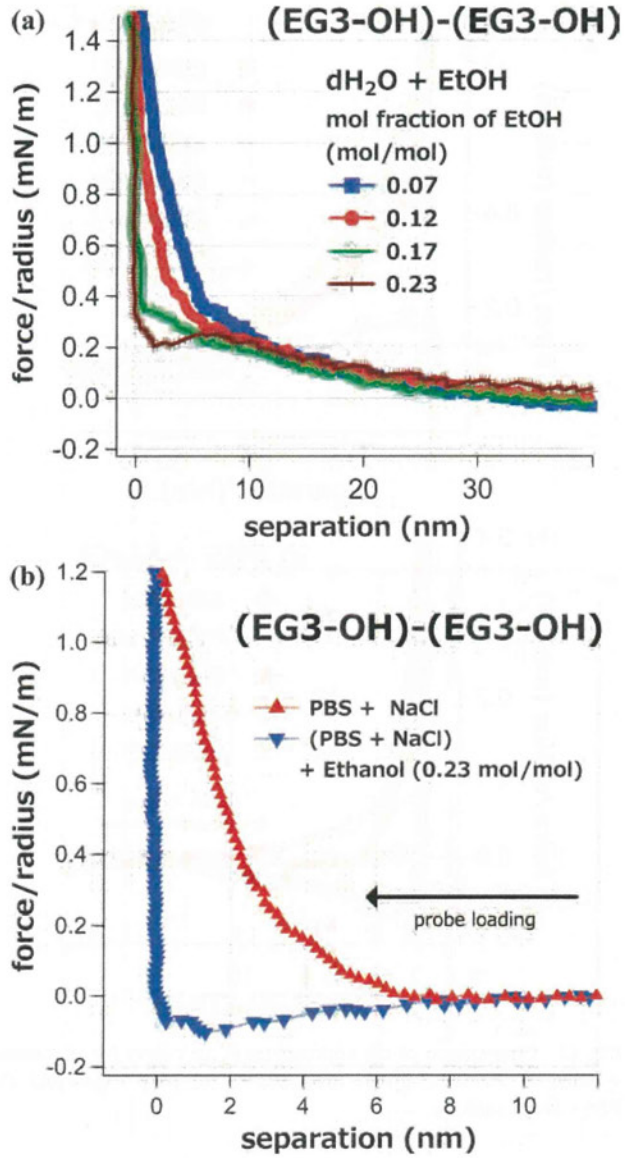

Fig. 14 Force *vs.* distance curves recorded on the approach of EG3–OH SAMs in mixtures of water (buffer) and ethanol: (a) in a mixture of pure water and ethanol, (b) in a mixture of buffer (PBS buffer pH 7.4, 10 mM containing NaCl at a concentration of 0.6 M) and ethanol. Note that only water was taken into consideration to calculate molar ratios (ions were not considered).

network of water takes place at P_{et} values higher than 0.2.[31,32] In our surface force measurements, the short-range repulsion disappeared at $P_{et} > 0.17$. By summing up the above discussions, we concluded that structured water molecules in the interfacial region with a thickness of 2–3 nm were responsible for the short-range repulsion.

The mechanical properties of the structured water were investigated by a simple Hertz model,

$$F = \frac{4\sqrt{R}}{3}\frac{E}{1-\nu^2}\delta^{3/2}. \quad (5)$$

where F, R, E, ν, and δ are the force, probe radius, elastic modulus, Poisson ratio (assumed to 0.5) and indentation. The fitting was carried out in a region where the repulsive force increased from zero and the fitting range was 1 to 1.5 nm (used as the parameter of the indentation). The obtained elastic moduli were 9 to 13 kPa for EG3–OH, 10 to 14 kPa for EG3–OMe, and 6 to 10 kPa for EG6–OH, which are comparable to the elastic moduli of relatively soft hydrated polymer gels [*e.g.* poly(vinyl alcohol)]. We anticipate that structured water molecules whose mechanical properties differ from those of bulk water act as a physical barrier for platelet adhesion.

Mechanism underlying the bioinertness of OEG-SAMs

The origin of the bioinertness of poly(ethylene glycol): PEG-grafted surfaces have been considered to be attributed to the elastic effect due to the flexibility of the PEG chains and the osmotic effect due to water molecules tightly bound to the PEG chains.[33] Considering the high density of molecules constituting the OEG-SAMs in this work (>81%) (Table 1), the elastic effect is too small to deter proteins and platelets from adhesion.

The computer simulation by Pertsin *et al.* was performed by assuming a packing density of 21.4 $Å^2$ per thiolate (ideal defect-free SAM of alkanethiols on Au(111)).[34,35] With this condition, the penetration of water into SAM was confirmed. The neutron reflectivity measurement by Schwendel *et al.* supported the fact of penetration of water into the SAM.[36] The simulation by Zheng *et al.* indicated that the penetration of water becomes significant with reducing molecular density.[13] In addition, Herrwerth *et al.* and Li *et al.* found that OEG-SAMs with high molecular density adsorb small amount of proteins.[14,15] Vanderah *et al.* also reported that BSA adsorbs on to the $HS(OCH_2CH_2)_6CH_3$ SAMs in which an ordered helical structure is dominant, whereas BSA did not adsorb the SAM with disordered molecular conformations.[37] Felipe *et al.* also reported a similar finding with the monolayers of (OEG)ylated carbazole linear dendrons formed on Au substrate.[38] The above reports clearly suggest that water molecules penetrate to OEG-SAMs and they are tightly bound to the EG units. The tightly-bound water molecules may contribute to the osmotic effect. The packing density of the OEG molecules in the monolayers in our work is lower than that of the ideal system (Table 1), indicating that the water molecules can be accommodated in the OEG-SAMs used in this work.

However, the range of the repulsion observed for the EG3–OH, EG3–OMe, and EG6–OH SAMs is 4–6 nm. This suggests that not only tightly-bound water molecules but also interfacial water molecules with a thickness of 2–3 nm (half of the range of the repulsion between the SAMs) cause the repulsion. Smith *et al.* investigated the structure and dynamics of water molecules in the vicinity of a chain of poly(ethylene glycol), and found that the water molecules formed clusters.[39] We expect that this clustering of water occurs at the interface of water and SAMs, since the intermixing of water and EG chains occurs because of the penetration of water into the SAM. The EG3–OH, EG3–OMe and EG6–OH SAMs possess a thick intermixing region (number of the EG units), resulting in the thick (2 to 3 nm) layer of structured interfacial water observed in the force measurement. In contrast, the EG1–OH and EG2–OH SAMs provide a small volume of intermixing region, resulting in the reduced thickness of the structured water (or only tightly-bound water molecules).

The number of EG units required for anti-platelet adhesion was at least three, whereas that required for the protein-resistance was one. We speculate that the cause of the discrepancy is the huge differences in the sizes and weights of protein molecules and platelets, which directly relates to the differences in the strengths of van der Waals interactions and the mobilities of protein molecules and platelets at the interface. A structured water layer with a small thickness (less than 1 nm) and water molecules strongly bound to the EG part, which may be the origin of the osmotic repulsion, suffices to prevent the adsorption of the proteins (5–50 nm in size). On the other hand, platelets tend to remain on the monolayers for longer because of their large size (2–3 μm) and strong van der Waals interaction with the monolayers. In addition, the extracellular matrix proteins are forced to remain in the confined region between platelet and monolayers, and the proteins as well as platelet must be repelled for antiplatelet adhesion. In such a case, the osmotic effect due to tightly-bound water alone is not enough and thick structured water layers are required to prevent platelet adhesion.

It is also necessary to mention that the thickness of the layer of the structured water near the OEG-SAMs is obviously different from that found for lipid bilayers and mica, as observed by non-contact AFM[40–42] and X-ray reflectometry.[43] In these previous reports, only two or three hydration layers were observed. However, the thickness of the water layer in the vicinity of the OEG-SAMs was far beyond that of these hydration structures and is highly unexpected. We anticipate that the structuring of the water observed in this work does not appear in their local density profiles, since the water structure is rather dynamic compared with tightly bound water observed with the above techniques. Our recent vibrational analysis of water in the vicinity of the SAM by attenuated total reflection Fourier transform infrared (ATR-FTIR) spectroscopy, which will be published elsewhere, revealed that the shapes of the O–H stretching bands of OEG-SAMs were obviously different from those of other SAMs (the CH_3, OH, NH_2 and COOH SAMs). This result may be key to understanding the structuring of the water found in this work.

Water-induced repulsion *vs.* electrostatic interaction

As presented in Fig. 2 and 5, the EG3–NH_2 and EG3–COOH SAMs significantly adsorbed the proteins and adhered platelets. To explain these results, there are two possibilities: 1. The structuring of water molecules does not occur because of the charged terminal groups. 2. Attractive electrostatic interaction between the charged groups of the SAMs and proteins overwhelms the water-induced repulsion. Fig. 15 shows the force–distance curves for the interactions between the symmetric systems of EG3–NH_2 and –COOH SAMs. It is clear that the ranges of the repulsion observed for both EG3–NH_2 and –COOH SAMs were much longer than those of the NH_2 and COOH SAMs. We also found that these repulsions observed for the EG3–NH_2 and –COOH SAMs in the PBS + NaCl solution did not appear in the mixture of ethanol and PBS + NaCl solution (P_{et} = 0.23) (data not shown). Therefore, we concluded that structured water molecules exist in the vicinity of the EG3–NH_2 and EG3–COOH SAMs. We speculate the following model for the cases of these SAMs.

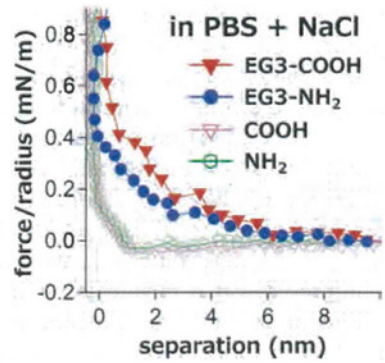

Fig. 15 Force–separation curves recorded on approach for symmetric systems of the SAMs (the same SAMs prepared for both probe and substrate) in PBS + NaCl solution.

The kinetic energy of the protein molecules in solution obeys the Maxwell–Boltzmann distribution law. Despite the existence of the barrier of the structured water, some protein molecules possessing high kinetic energy can hop over the barrier and adsorb onto the SAMs *via* local electrostatic interaction between charges carried by proteins and the SAMs, which also results in platelet adhesion.

The values of $\Delta d/\Delta f$ values obtained by QCM (Fig. 4) show that the proteins adsorbed on the EG3–NH_2 and EG3–COOH SAMs were softer than those adsorbed on the NH_2 and COOH SAMs. We expect the following situation: the protein molecules interact with the EG3–NH_2 and EG3–COOH SAMs *via* local interaction between the charged groups of the protein and SAMs, and the structured water molecules still exist around the adsorbed proteins. As a result, the protein molecules can maintain their native shapes, resulting in large $\Delta d/\Delta f$ values. By contrast, the NH_2 and COOH SAMs provide more sites to the protein molecules' electrostatic interaction between the charged groups of the protein and SAMs, which may induce significant denaturation of the proteins, resulting in the small $\Delta d/\Delta f$ values because of the absence of the structured water layer. Therefore, for the immobilization of protein molecules onto solid surfaces without loss of their functions, the molecules making up the substrate should contain OEG moieties.

Conclusions

In this work, we performed systematic analyses of protein absorption, platelet adhesion, and surface forces of SAMs with various terminal groups. Our force measurements of the interaction between OEG-SAMs revealed that structured water molecules exist at the SAM–water interface when the constituting thiol molecules possess more than two EG units. Our results showed that at least one EG unit is necessary for protein resistance, whereas three EG units are required to endow the SAMs with platelet compatibility. It was found that the SAMs that exhibited the water-mediated repulsion in the surface force measurements also deterred platelet adhesion, indicating that a physical barrier of water molecules with a thickness of 2 to 3 nm is necessary for the anti-platelet adhesion. On the other hand, only a thin layer of structured water or tightly bound water was found to be required for the protein resistance. We also found that the charge neutrality of

the terminal groups of the SAMs is essential for their protein resistance and platelet compatibility. Our result also indicates that structuring of the interfacial water occurs even when the thiol molecules possess charged groups as well as EG groups (EG3–NH_2 and EG3–COOH). In such a case, however, the local electrostatic interaction between the protein and SAM overwhelms the water-induced repulsion, resulting in the adsorption of proteins and the adhesion of platelets.

We hope that our findings will help in the design of novel biomaterials, in processes that require the immobilization of biomolecules without loss of their native function, and in new understanding of the mechanisms underlying specific molecular recognition in biological systems.

Acknowledgements

We thank Prof. Michael Grunze (University of Heidelberg) for stimulating and fruitful discussions. Professor Emeritus Teiji Tsuruta (University of Tokyo) is gratefully acknowledged for his critical and helpful comments on this work. Part of this work was supported by Grant-in-Aid for Young Researchers (B) from MEXT.

References

1 T. Hayashi and M. Hara, *Curr. Phys. Chem.*, 2011, **1**, 90–98.
2 K. L. Prime and G. M. Whitesides, *Science*, 1991, **252**, 1164–1167.
3 K. L. Prime and G. M. Whitesides, *J. Am. Chem. Soc.*, 1993, **115**, 10714–10721.
4 R. Ogaki, M. Alexander and P. Kingshott, *Mater. Today*, 2010, **13**, 22–35.
5 B. Liedberg and T. Ekblad, *Curr. Opin. Colloid Interface Sci.*, 2010, **15**, 499–509.
6 Y. H. M. Chan, R. Schweiss, C. Werner and M. Grunze, *Langmuir*, 2003, **19**, 7380–7385.
7 S. Schilp, A. Kueller, A. Rosenhahn, M. Grunze, M. E. Pettitt, M. E. Callow and J. A. Callow, *Biointerphases*, 2007, **2**, 143–150.
8 C. Christophis, M. Grunze and A. Rosenhahn, *Phys. Chem. Chem. Phys.*, 2010, **12**, 4498–4504.
9 A. Rosenhahn, S. Schilp, H. J. Kreuzer and M. Grunze, *Phys. Chem. Chem. Phys.*, 2010, **12**, 4275–4286.
10 H. I. Kim, J. G. Kushmerick, J. E. Houston and B. C. Bunker, *Langmuir*, 2003, **19**, 9271–9275.
11 S. F. Chen, J. Zheng, L. Y. Li and S. Y. Jiang, *J. Am. Chem. Soc.*, 2005, **127**, 14473–14478.
12 Y. He, Y. Chang, J. C. Hower, J. Zheng, S. F. Chen and S. Jiang, *Phys. Chem. Chem. Phys.*, 2008, **10**, 5539–5544.
13 J. Zheng, L. Y. Li, S. F. Chen and S. Y. Jiang, *Langmuir*, 2004, **20**, 8931–8938.
14 S. Herrwerth, W. Eck, S. Reinhardt and M. Grunze, *J. Am. Chem. Soc.*, 2003, **125**, 9359–9366.
15 L. Y. Li, S. F. Chen, J. Zheng, B. D. Ratner and S. Y. Jiang, *J. Phys. Chem. B*, 2005, **109**, 2934–2941.
16 K. Feldman, G. Hahner, N. D. Spencer, P. Harder and M. Grunze, *J. Am. Chem. Soc.*, 1999, **121**, 10134–10141.
17 C. Dicke and G. Hahner, *J. Am. Chem. Soc.*, 2002, **124**, 12619–12625.
18 C. Dicke and G. Hahner, *J. Phys. Chem. B*, 2002, **106**, 4450–4456.
19 B. Lüssem, S. Karthauser, H. Haselier and R. Waser, *Appl. Surf. Sci.*, 2005, **249**, 197–202.
20 D. G. Castner, K. Hinds and D. W. Grainger, *Langmuir*, 1996, **12**, 5083–5086.
21 T. Hayashi, K. Wakamatsu, E. Ito and M. Hara, *J. Phys. Chem. C*, 2009, **113**, 18795–18799.
22 C. Fredriksson, S. Khilman, B. Kasemo and D. M. Steel, *J. Mater. Sci.: Mater. Med.*, 1998, **9**, 785–788.
23 F. Hook, B. Kasemo, T. Nylander, C. Fant, K. Sott and H. Elwing, *Anal. Chem.*, 2001, **73**, 5796–5804.
24 A. Agnihotri and C. A. Siedlecki, *Langmuir*, 2004, **20**, 8846–8852.
25 R. E. Marchant and P. S. Sit, *Thromb.Haemostasis*, 1999, **82**, 1053–1060.
26 R. E. Marchant and P. S. Sit, *Surf. Sci.*, 2001, **491**, 421–432.
27 M. Tanaka, T. Motomura, M. Kawada, T. Anzai, Y. Kasori, T. Shiroya, K. Shimura, M. Onishi and A. Mochizuki, *Biomaterials*, 2000, **21**, 1471–1481.
28 B. Sivaraman and R. A. Latour, *Biomaterials*, 2010, **31**, 832–839.
29 J. Israelachvili, *Intermolecular and Surface Forces*, Academic Press, London, 1992.
30 H. J. Butt, B. Cappella and M. Kappl, *Surf. Sci. Rep.*, 2005, **59**, 1–152.
31 Z. X. Li, J. R. Lu, D. A. Styrkas, R. K. Thomas, A. R. Rennie and J. Penfold, *Mol. Phys.*, 1993, **80**, 925–939.
32 M. Matsumoto, N. Nishi, T. Furusawa, M. Saita, T. Takamuku, M. Yamagami and T. Yamaguchi, *Bull. Chem. Soc. Jpn.*, 1995, **68**, 1775–1783.
33 S. I. Jeon, J. H. Lee, J. D. Andrade and P. G. Degennes, *J. Colloid Interface Sci.*, 1991, **142**, 149–158.
34 A. J. Pertsin and M. Grunze, *Langmuir*, 2000, **16**, 8829–8841.
35 A. J. Pertsin, T. Hayashi and M. Grunze, *J. Phys. Chem. B*, 2002, **106**, 12274–12281.
36 D. Schwendel, T. Hayashi, R. Dahint, A. Pertsin, M. Grunze, R. Steitz and F. Schreiber, *Langmuir*, 2003, **19**, 2284–2293.
37 D. J. Vanderah, G. Valincius and C. W. Meuse, *Langmuir*, 2002, **18**, 4674–4680.
38 M. J. Felipe, P. Dutta, R. Pernites, R. Ponnapati and R. C. Advincula, *Polymer*, 2012, **53**, 427–437.
39 G. D. Smith, D. Bedrov and O. Borodin, *Phys. Rev. Lett.*, 2000, **85**, 5583–5586.
40 K. Kimura, S. Ido, N. Oyabu, K. Kobayashi, Y. Hirata, T. Imai and H. Yamada, *J. Chem. Phys.*, 2010, **132**, 194705–194709.
41 T. Fukuma, *Sci. Technol. Adv. Mater.*, 2010, **11**, 033003–033020.
42 T. Fukuma, M. J. Higgins and S. P. Jarvis, *Biophys. J.*, 2007, **92**, 3603–3609.
43 L. Cheng, P. Fenter, K. L. Nagy, M. L. Schlegel and N. C. Sturchio, *Phys. Rev. Lett.*, 2001, **87**, 156103–156106.

Synthesis of Graft Copolymers Based on Poly(2-Methoxyethyl Acrylate) and Investigation of the Associated Water Structure

Irakli Javakhishvili, Masaru Tanaka, Keiko Ogura, Katja Jankova, Søren Hvilsted*

Graft copolymers composed of poly(2-methoxyethyl acrylate) are prepared employing controlled radical polymerization techniques. Linear backbones bearing atom transfer radical polymerization (ATRP) initiating sites are obtained by reversible addition–fragmentation chain transfer copolymerization of 2-methoxyethyl acrylate (MEA) and 2-(bromoisobutyryloxy)ethyl methacrylate (Br^{i}BuEMA) as well as 2-hydroxyethyl methacrylate and Br^{i}BuEMA in a controlled manner . MEA is then grafted from the linear macroinitiators by Cu (I)-mediated ATRP. Fairly high molecular weights (>120 000 Da) and low polydispersity indices (1.17–1.38) are attained. Thermal investigations of the graft copolymers indicate the presence of the freezing bound water, and imply that the materials may exhibit blood compatibility.

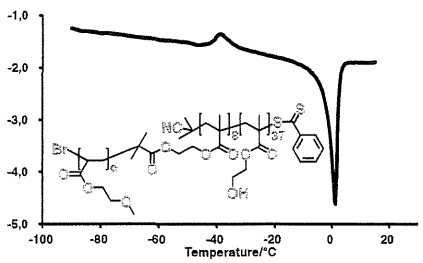

1. Introduction

Polymeric materials intended for medical devices that may come in contact with blood should display capacity to resist protein adsorption and blood cell adhesion and thus triggering the organism's defense mechanism. Numerous blood compatible surfaces have been developed, and they fall into the following three categories: hydrophilic surfaces, surfaces with microphase-separated domains, and biomembrane-like surfaces. Alongside myriads of physicochemical properties including surface charge, wettability, surface free energy, topography, stiffness, and the presence of specific chemical functionalities, surface-bound water appears to bear an instrumental role in the biological response induced by the artificial material.[1]

Dr. I. Javakhishvili, Assoc. Prof. K. Jankova, Prof. S. Hvilsted
Danish Polymer Centre, Department of Chemical and Biochemical Engineering, Technical University of Denmark, Søltofts Plads, Building 227, Kongens Lyngby 2800, Denmark
E-mail: sh@kt.dtu.dk
Prof. M. Tanaka, K. Ogura
Department of Biochemical Engineering, Graduate School of Science and Technology, Yamagata University, Yonezawa 992-8510, Japan

Poly(2-methoxyethyl acrylate) (PMEA) displays excellent blood compatibility, and has been approved for medical use by the FDA.[1] For instance, PMEA-coated circuits exhibit significantly reduced complement activation when used in cardiopulmonary bypass.[2] It has been maintained that PMEA's compatibility with platelet, white blood cells, complement and coagulation systems has been dictated by the presence of the freezing bound water.[1] Attempts have been made to shed light on the water structure in PMEA, and its influence on the blood compatibility. Thus, random[1a] and block[1b] copolymers of 2-methoxyethyl acrylate (MEA) and 2-hydroxyethyl methacrylate (HEMA) have been synthesized by free radical and anionic polymerization techniques, respectively, and the effect of the monomer composition and the copolymer topology has been elucidated. However, necessity of meticulous investigations of the blood compatibility mechanism demands precise synthesis of more advanced macromolecular architectures comprising MEA in combination with HEMA or other hydrophilic monomers. This contribution details the synthetic approach, structural, and thermal characterization of graft copolymers based on MEA and HEMA. Because controlled radical polymerization (CRP) techniques such as atom transfer radical polymerization (ATRP)[3] and reversible addition–fragmentation chain transfer (RAFT)

Macromol. Rapid Commun. **2012**, DOI: 10.1002/marc.201100698

polymerization[4] have emerged as versatile, robust, and resourceful tools for building complex macromolecular structures with virtually innumerable combinations of monomers, initiating and catalytic systems, we decided to marry the two for preparation of well-defined graft copolymers featuring PMEA or poly(2-hydroxyethyl methacrylate) (PHEMA) backbones and PMEA grafts. Copolymerization of MEA with acrylonitrile (AN) by copper (I)-mediated ATRP together with extensive NMR spectroscopy studies was reported by Brar and Saini.[5] Our group has carried out exhaustive investigations covering polymerization kinetics of copper (I)-catalyzed ATRP of MEA as well as end-group analysis and chain extension reaction to obtain block copolymers of PMEA while probing different catalytic complexes, reaction milieu, and temperature.[6] Coelho et al.[7] obtained PMEA by single electron transfer-degenerative transfer radical polymerization; however, the molecular weight distributions (MWD) were rather broad. PMEA and random copolymers of MEA with 2-hydroxyethyl acrylate were prepared by RAFT and nitroxide-mediated homo- and copolymerization, respectively, and the thermoresponsive properties of these materials were assessed.[8] Employing trithiocarbonate RAFT agent resulted in the formation of azeotropic copolymers. Polymeric trithiocarbonate chain transfer agent (CTA) was utilized in solution as well as dispersion RAFT polymerization of MEA with fairly good control.[9]

Matyjaszewski and co-workers[10] reported preparation of graft copolymers by two sequential ATRP steps and by combining free radical polymerization and ATRP. The former approach involved ATRP of trimethylsilyl-protected HEMA followed by transformation of the hydroxyl groups along the polymer backbone to the ATRP initiating sites by treating them with 2-bromoisobutyryl bromide (Br^{i}BuBr), and ATRP of styrene (St) and butyl acrylate. The latter approach consisted of free radical polymerization of 2-(2-bromopropionyloxy)ethyl acrylate (BrPrEA) followed by ATRP. In a similar fashion, block and random copolymers of AN and HEMA were synthesized by RAFT (co) polymerization making use of a dithioester CTA.[11] The hydroxyl functions were then converted into the ATRP initiating moieties by reacting with Br^{i}BuBr. These macroinitiators were successfully employed in ATRP of *N*-isopropylacrylamide. However, it would be advantageous to eliminate the intermediate steps related to the incorporation of initiating sites along a polymer backbone. Klumperman and co-workers[12] carried out well-controlled RAFT (co)polymerization of 2-(bromoisobutyryloxy)ethyl methacrylate (Br^{i}BuEMA) utilizing 2-cyano-2-propyl benzodithioate (CPBdT) as the CTA. Relatively narrow MWD and symmetrical size exclusion chromatography (SEC) traces were reported. Thus, well-defined macromolecular scaffolds with multiple ATRP initiating functions were prepared while circumventing protective group chemistry and demanding purification steps.[12] Graft and star graft copolymers were constructed in a similar manner: RAFT polymerizations of BrPrEA or *tert*-butyl 2-((2-bromopropanoyloxy)methyl) acrylate were followed by grafting of hydrophobic as well as hydrophilic monomers from the linear backbones by ATRP or grafting poly(propylene oxide) chains to the star arms or linear chains by atom transfer or single electron transfer nitroxide radical coupling.[13]

In the present work, the linear precursors for the graft copolymers were built by RAFT copolymerization of MEA with Br^{i}BuEMA and HEMA with Br^{i}BuEMA employing a dithioester—CPBdT—as a CTA. Fairly narrow MWDs were attained. MEA was then grafted from these multifunctional macroinitiators by copper (I)-mediated ATRP. Well-defined graft copolymers were obtained, and subjected to scrupulous investigations to uncover the traits responsible for the blood compatibility. We found that the hydrated graft copolymers possessed a unique water structure, observed as cold crystallization of water. To the best of our knowledge, no such combination of the monomers and macromolecular architecture has been reported before.

2. Experimental Section

2.1. Materials

2-Methoxyethyl acrylate (MEA; Aldrich, 98%) and 2-hydroxyethyl methacrylate (HEMA; Aldrich, 99% +) were passed through short aluminum oxide columns (Sigma-Aldrich, activated, basic, Brockmann I, standard grade, ≈150 mesh, 58 Å) before being used. Toluene (Sigma-Aldrich, 99.9%) and tetrahydrofuran (THF; Sigma-Aldrich, 99.9%) were dried over CaH_2 and distilled under nitrogen flow. Triethylamine (Fluka, ≥ 98%) was distilled under nitrogen flow. 2-Bromoisobutyryl bromide (Br^{i}BuBr; Aldrich, 98%), *N,N*-dimethylformamide (DMF; Sigma-Aldrich, ≥ 99.9%), anisole (Sigma-Aldrich, 99%), methanol (Sigma-Aldrich, 99.9%), heptane (Sigma-Aldrich, 99%), dichloromethane (Sigma-Aldrich, 99.8%), chloroform (Sigma-Aldrich, 99.8%), 4-(dimethylamino)pyridine (4-DMAP; Fluka, >98%), CuBr (Sigma-Aldrich, 98%), 2-cyano-2-propyl benzodithioate (CPBdT; Aldrich, >97%), 1,1,4,7,10,10-hexamethyltriethylenetetramine (HMTETA; Aldrich, 97%), *N,N,N′,N″,N″*-pentamethyldiethylenetriamine (PMDETA; Aldrich, 99%), $CDCl_3$ (Aldrich, 99.8 atom% D), and dimethyl sulfoxide (DMSO)-d_6 (Aldrich, 99.9 atom% D) were used as received. 2,2′-Azobis(2-methylpropionitrile) (AIBN; from Ventron) was recrystallized from MeOH.

2.2. Analytical Techniques

NMR spectroscopy experiments were conducted on a Bruker Avance 300 MHz spectrometer. The coupling constants are given in Hz while chemical shifts are given in ppm. Molecular weights and polydispersity index (PDI) were estimated by size exclusion

Macromol. Rapid Commun. 2012, DOI: 10.1002/marc.201100698

chromatography (SEC) using the following instrument: Viscotek GPCmax VE-2001 equipped with Viscotek TriSEC Model 302 triple detector array (refractive index detector, viscometer detector, and laser light scattering detector with the light wavelength of 670 nm, and measuring angles of 90° and 7°) and a Knauer K-2501 UV detector using two PLgel mixed-D columns from Polymer Laboratories (PL). The samples were run in THF at 30 °C (1 mL min^{-1}). Molecular weights were calculated using polystyrene (PS) standards from PL. Thermogravimetric analysis (TGA) was performed on a TGA Q500 instrument from 20 to 800 °C with a heating rate of 20 °C min^{-1} under nitrogen flow.

The phase transitions of water in the polymer were measured by differential scanning calorimetry (DSC) (Thermo Plus 8230, Rigaku, Japan) equipped with a low-temperature cooling apparatus. The sample was placed in an aluminum pan and hermetically sealed. The weight of the sample was 3–4 mg. The sample was first cooled down to −100 °C at the rate of 5.0 °C min^{-1}, held at −100 °C for 5 min, and then heated to 50 °C at the same rate under a nitrogen atmosphere. The heating process was monitored. It was confirmed that there was no weight loss during the measurement.

Water content of the polymer was defined by the following equation:

Water content (wt%) = $\{(W1 - W0)/W1\} \times 100$, where $W0$ and $W1$ are the weights of the dry sample and the hydrated sample, respectively. The water content was then obtained by the method described below: The polymer sample was soaked in distilled water for 7 d at room temperature, taken out of water, and wiped with a filter paper to remove excess water on the surface. The fully hydrated polymer was weighed quickly ($W1$), and then the polymer was dried at 120 °C in vacuo until the weight ($W0$) became constant.

2.3. Synthetic Procedures

All reactions were conducted under a nitrogen atmosphere.

2-(Bromoisobutyryloxy)ethyl methacrylate (Br^{i}BuEMA): HEMA (9.5 mL, 78.3 mmol), 4-DMAP (5.68 g, 38.3 mmol), and NEt_3 (27 mL, 193.7 mmol) were placed in a 250 mL two-neck round bottom flask equipped with a magnetic stirring bar, a rubber septum, and an addition funnel, and were dissolved in THF (145 mL). The reaction mixture was cooled on ice/water bath, and Br^{i}BuBr (19 mL, 153.7 mmol) was added dropwise. The reaction was carried out overnight at room temperature. Afterward, the mixture was filtered, concentrated in vacuo, and dissolved in $CHCl_3$. It was then extracted with dilute aqueous $NaHCO_3$ (7 × 130 mL), dilute aqueous $NaHSO_4$ (3 × 130 mL), and distilled water (1 × 100 mL). The solution was dried with anhydrous $MgSO_4$, filtered, and concentrated under reduced pressure. It was then redissolved in MeOH (200 mL), chilled in a freezer, and extracted with heptane (7 × 200 mL). Heptane was removed under reduced pressure, and the product was dissolved in CH_2Cl_2 (150 mL). The solution was washed, dried, and concentrated as described above resulting in a yield of 62.6%.

^{1}H NMR (300 MHz, $CDCl_3$, δ): 6.12 (s, 1H, CH_2=C), 5.58 (s, 1H; CH_2=C), 4.40 (m, 4H; CH_2), 1.80–2.10 (m, 9H, CCH_3 and $CBr(CH_3)_2$).

General Procedure for RAFT Copolymerization: A previously dried Schlenk tube was charged with Br^{i}BuEMA and MEA or HEMA, AIBN, CPBdT, and toluene or DMF. Three freeze–pump–thaw cycles were performed, and the tube was immersed into preheated oil bath at 70 °C. The copolymerization reaction was monitored by SEC, and was quenched with liquid nitrogen. The reaction mixture was diluted with THF, and precipitated twice into heptane or Et_2O-heptane (1:1) mixture at room temperature. Pink precipitate was isolated and dried in the vacuum oven at room temperature. The degree of polymerization (DP) and composition of the copolymer were estimated by ^{1}H NMR experiment, while the PDI was obtained by SEC using the PS calibration curve.

Poly(2-(Bromoisobutyryloxy)ethyl methacrylate)-co-2-methoxyethyl acrylate) (P(Br^{i}BuEMA-co-MEA)). Br^{i}BuEMA (0.7 mL, 3.5 mmol), MEA (2.4 mL, 18.7 mmol), AIBN (16 mg, 0.1 mmol), CPBdT (76 mg, 0.34 mmol), and toluene (3.5 mL) were employed. The polymerization time was 4.5 h. $\overline{M}_n$(^{1}H NMR) = 5900 Da, DP of Br^{i}BuEMA was 9, DP of MEA was 23; $\overline{M}_n$(SEC) = 5700 Da, $\overline{M}_w$(SEC) = 7400 Da, $\overline{M}_w/\overline{M}_n$ = 1.29. ^{1}H NMR (300 MHz, DMSO-d_6, δ): 7.83–8.00 (b, 2H, *m*, -Ar), 7.61–7.77 (b, 1H; *p*, -Ar), 7.42–7.58 (b, 2H; *o*, -Ar), 4.26–4.50 (b, $C(CH_3)C(O)OCH_2$), 3.85–4.26 (b, $HCC(O)OCH_2$, and $C(CH_3)_2C(O)OCH_2$) (resonances over the range of 3.85–4.50 ppm correspond to 82 H), 3.38–3.68 (b, 46 H, CH_3OCH_2), 3.14–3.30 (b, 69 H, CH_3O), 2.08–2.42 (b, 23 H, $CH_2CHC(O)O$), 1.90 (s, $BrC(CH_3)_2$), 0.75–2.08 (b, $CH_2C(CH_3)C(O)O$, $CH_2C(CH_3)C(O)O$, and $CH_2CHC(O)O$) (0.75–2.08 corresponds to 145 H).

Poly(2-(Bromoisobutyryloxy)ethyl methacrylate)-co-2-hydroxyethyl methacrylate) (P(Br^{i}BuEMA-co-HEMA)). Br^{i}BuEMA (0.7 mL, 3.5 mmol), HEMA (2.1 mL, 17.3 mmol), AIBN (15.6 mg, 0.1 mmol), CPBdT (76 mg, 0.34 mmol), and DMF (3.5 mL) were taken. The reaction was terminated after 3 h. $\overline{M}_n$ (^{1}H NMR) = 7300 Da, DP of Br^{i}BuEMA was 8, DP of HEMA was 37; $\overline{M}_n$(SEC) = 3700 Da, $\overline{M}_n$(SEC) = 5500 Da, $\overline{M}_w/\overline{M}_n$ = 1.47. ^{1}H NMR (300 MHz, DMSO-d_6, δ): 7.73–7.88 (b, 2H, *m*, -Ar), 7.57–7.70 (b, 1H; *p*, -Ar), 7.35–7.55 (b, 2H; *o*, -Ar), 4.80 (b, 37 H, CH_2OH), 4.25–4.55 (b, $CH_2C(CH_3)C(O)OCH_2$), 4.03–4.25 (b, $C(CH_3)_2C(O)OCH_2$), 3.72–4.03 (b, $C(O)OCH_2CH_2OH$) (3.72–4.55 corresponds to 106 H), 3.43–3.72 (b, 74 H, CH_2OH), 1.93 (b, $BrC(CH_3)_2$), 0.40–2.20 (b, $CH_2C(CH_3)C(O)O$ and $CH_2C(CH_3)C(O)O$) (0.40–2.20 accounts for 273 H).

General Procedure for ATRP: The macroinitiator P(Br^{i}BuEMA$_9$-*co*-MEA$_{23}$) or P(Br^{i}BuEMA$_8$-*co*-HEMA$_{37}$), MEA, CuBr, DMF, and anisole were introduced into a Schlenk tube, and two freeze–pump–thaw cycles were performed. Then PMDETA was injected, and two freeze–pump–thaw cycles were carried out. The polymerization was conducted at 70 °C in bulk or at 90 °C in solution. The graft copolymer was precipitated in Et_2O, and dried in the vacuum oven at room temperature. The molecular weight and the MWD were obtained by SEC employing the light scattering detector (dn/dc = 0.060).[7]

P(Br^{i}BuEMA$_9$-co-MEA$_{23}$)-g-PMEA: P(Br^{i}BuEMA$_9$-*co*-MEA$_{23}$) (52 mg, 0.08 mmol of the initiating sites), MEA (5 mL, 38.9 mmol), CuBr (8.2 mg, 0.06 mmol), and PMDETA (10 μL, 0.05 mmol) were charged. The reaction was quenched in 15 min. $\overline{M}_n$(SEC) = 23 000 Da, $\overline{M}_n$(SEC) = 29 300 Da, $\overline{M}_w/\overline{M}_n$ = 1.27.

P(Br^{i}BuEMA$_9$-co-MEA$_{23}$)-g-PMEA. P(Br^{i}BuEMA$_9$-*co*-MEA$_{23}$) (49 mg, 0.075 mmol of the initiating sites), MEA (5 mL, 38.9 mmol), CuBr (17 mg, 0.12 mmol), PMDETA (25 μL, 0.12 mmol), DMF (5 mL), and anisole (5 mL) were taken. The polymerization was allowed

to proceed for 30 min. $\overline{M}_n$(SEC) = 131 300 Da, $\overline{M}_w$(SEC) = 181 700 Da, $\overline{M}_w/\overline{M}_n$ = 1.38.

P(Br^{i}BuEMA$_8$-co-HEMA$_{37}$)-g-PMEA: P(Br^{i}BuEMA$_8$-*co*-HEMA$_{37}$) (51 mg, 0.056 mmol of the initiating sites), MEA (3.6 mL, 28.0 mmol), CuBr (12.9 mg, 0.09 mmol), PMDETA (14 μL, 0.07 mmol), DMF (3.6 mL), and anisole (3.6 mL) were used. The polymerization was carried out for 30 min. $\overline{M}_n$(SEC) = 120 300 Da, $\overline{M}_n$(SEC) = 140 400 Da, $\overline{M}_w/\overline{M}_n$ = 1.17.

3. Results and Discussion

3.1. Preparation of Multifunctional Linear Macroinitiators

Synthesis of linear copolymers incorporating MEA and Br^{i}BuEMA, and HEMA and Br^{i}BuEMA was carried out as depicted in Scheme 1. Initially, a methacrylic monomer possessing an ATRP initiating site—Br^i BuEMA—was obtained by reacting HEMA with Br^{i}BuBr in the presence of a catalytic amount of 4-DMAP as opposed to the procedure reported earlier.[12] RAFT copolymerization of MEA and Br^{i}BuEMA was conducted in toluene using AIBN as the initiator and CPBdT as the CTA ($[M]_0:[I]_0:[CTA]_0$ = 222:1:3.4, M and I designate the monomer and initiator, respectively). That copolymerization of the acrylic and methacrylic monomers in the presence of the dithioester-type CTA proceeded in a controlled manner was substantiated by the low PDI of the copolymer as well as symmetrical and unimodal SEC traces (Figure 1A). ^{1}H NMR spectroscopy further verified formation of the copolymer by the RAFT process because the resonance peaks characteristic to the benzodithioate residue were observed in the range of 7.40–8.00 ppm (Figure S1, Supporting Information). This terminal aromatic tag was utilized to estimate the copolymer composition to be P(Br^{i}BuEMA$_9$-*co*-MEA$_{23}$). HEMA and Br^{i}BuEMA were copolymerized under similar conditions except that DMF was taken as the reaction medium (Table 1). The composition of P(Br^{i}BuEMA$_8$-*co*-HEMA$_{37}$) was determined by ^{1}H NMR spectroscopy (Figure 1B; Figure S2, Supporting Information). The SEC trace was monomodal, but exhibited tailing due to the interaction with the SEC columns when using THF as the eluent (Figure 1A). On the contrary, the analysis of P(Br^{i}BuEMA$_8$-*co*-HEMA$_{37}$) by SEC employing DMF + 0.05 M LiCl as the eluent furnished monomodal and symmetrical trace (Figure S3, Supporting Information). The molecular weight characteristics of the two copolymers are summarized in Table 1.

3.2. Preparation of Graft Copolymers

Grafting of MEA from the well-defined linear P(Br^{i}BuEMA$_9$-*co*-MEA$_{23}$) and P(Br^{i}BuEMA$_8$-*co*-HEMA$_{37}$) chains was accomplished by copper (I)-catalyzed ATRP. Homopolymerization of MEA mediated by CuBr/HMTETA and CuBr/PMDETA catalytic complexes in bulk and in toluene was thoroughly investigated by our group.[6] Initially, the reactions were carried out in DMF/anisole (1:1) mixture at 90 °C by making use of the CuBr/HMTETA catalytic system. The choice of solvents was dictated by the solubility of the P(Br^{i}BuEMA$_8$-*co*-HEMA$_{37}$) macroinitiator. Under these reaction conditions, ATRP proceeded rapidly, and resulted into the graft copolymers of rather large molecular weights and broad MWDs. This was attributed to the interchain coupling reactions facilitated by the prolonged reaction times and fairly low $[M]_0:[I]_0$ = 200 ratio. However, no insoluble fractions were observed. After few alterations in the experimental parameters, the protocols presented in Table 1 were adopted. Thus, the ATRP was conducted in solution at 90 °C or in bulk at 70 °C. The reaction times were shortened significantly, whereas the ratio of the initial

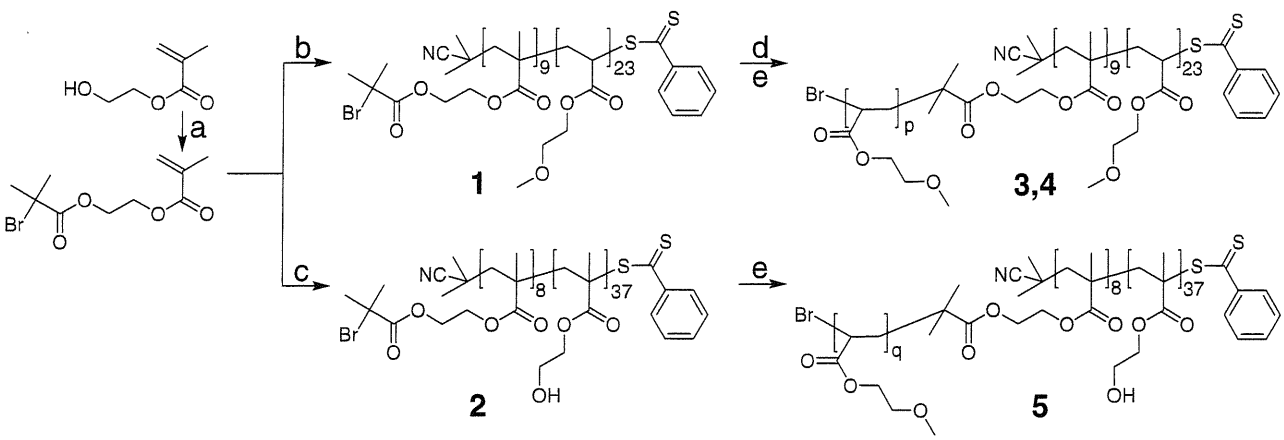

Scheme 1. Synthetic layout for preparation of the linear copolymers bearing ATRP initiating sites, and the corresponding graft copolymers. Reagents and conditions: (A) Br^i BuBr, 4-DMAP, NEt_3, THF; (B) MEA, AIBN, CPBdT, toluene, 70 °C; (C) HEMA, AIBN, CPBdT, DMF, 70 °C; (D) MEA, CuBr, PMDETA, bulk, 70 °C; (E) MEA, CuBr, PMDETA, DMF, anisole, 90 °C.

Macromol. Rapid Commun. 2012, DOI: 10.1002/marc.201100698

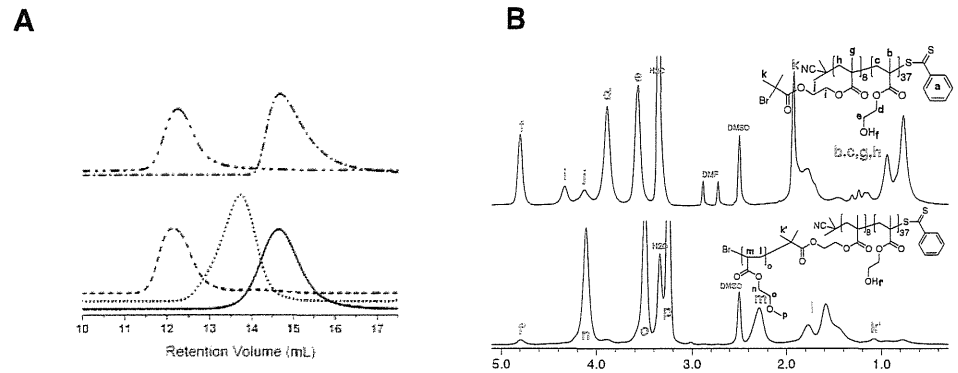

Figure 1. (A) An overlay of the SEC traces of the linear macroinitiators and the graft copolymers obtained thereof: P(Br^i BuEMA$_9$- *co* -MEA$_{23}$) (—), P(Br^i BuEMA$_9$-*co*-MEA$_{23}$)-*g*-PMEA (bulk) (···), P(Br^i BuEMA$_9$-*co*-MEA$_{23}$)-*g*-PMEA (—), P(Br^i BuEMA$_8$-*co*-HEMA$_{37}$) (–·), P(Br^i BuEMA$_8$-*co* -HEMA$_{37}$)-*g*-PMEA (–··). (B) An overlay of ^{1}H NMR spectra of P(Br^i BuEMA$_8$-*co*-HEMA$_{37}$) and P(Br^i BuEMA$_8$-*co*-HEMA$_{37}$)-*g*-PMEA emphasizing the high macroinitiator efficiency corroborated by the upfield shift of **k** (the chemical shifts are given in ppm).

molar concentration of the monomer to initiator was increased to about 500. When in bulk, the polymerization was catalyzed by 0.75 equivalents of CuBr and the reaction temperature was lowered to 70 °C to diminish the radical concentration, and thus suppress the coupling reactions.[10] High macroinitiator efficiency and fairly good control over the polymerization were achieved under these circumstances as indicated by the SEC experiments: the SEC traces were shifted to the lower elution volumes; they were unimodal and symmetrical, and only a small amount of a low molecular weight fraction was left when P(Br^{i}BuEMA$_9$-*co*-MEA$_{23}$) was employed as the macroinitiator (Figure 1A); low PDIs were obtained (Table 1). Graft copolymers of rather high molecular weights yet free from the coupling reaction products were prepared (Table 1, entries **4** and **5**). Moreover, PMEA grafts of different lengths could be synthesized by tuning the reaction parameters (Table 1, entries **3** and **4**). The overlay of the ^{1}H NMR spectra (Figure 1B) unequivocally confirms successful grafting from the P(Br^{i}BuEMA$_8$-*co*-HEMA$_{37}$) backbone. While the resonance signals originating from the linear precursor are dominated by the peaks arising from the grafted chains, **f′**, **m**, and **p** resonances (Figure 1B) suggest that the graft copolymer is indeed composed of PHEMA and PMEA segments. On the other hand, upfield shift of the resonance signal **k**, which corresponds to the methyl groups at the ATRP initiating sites, from 1.93 ppm (**k**) to 1.1 ppm (**k′**) indicates high macroinitiator efficiency in ATRP reactions.

TGA analysis reveals that the graft copolymers are stable until as high a temperature as 300 °C and the loss of only a minor fraction is observed before that (Figure S5, Supporting Information).

3.3. Investigation of the Water Structure by DSC

Thermal investigations of the water structure in a series of (meth)acrylic polymers revealed that linear PMEA featured unique water which underwent cold crystallization—a

Table 1. Reaction conditions, composition, and the molecular weight characteristics of the linear precursors and graft copolymers.

Entry	Linear and graft copolymers[a)]	Reagent ratio	Medium	Temp. [°C]	Time [min]	M_n [Da]	M_w [Da]	M_w/M_n
1[b)]	P(Br^i BuEMA$_9$- *co* -MEA$_{23}$)	220:1:3.4[d)]	Toluene	70	270	5700; 5900[a)]	7400	1.29
2[b)]	P(Br^i BuEMA$_8$- *co* -HEMA$_{37}$)	210:1:3.4[d)]	DMF	70	180	3700; 7300[a)]	5500	1.47
3[c)]	P(Br^i BuEMA$_9$-*co*-MEA$_{23}$)-*g*-PMEA	490:1:0.75:0.6[e)]	Bulk	70	15	23 000	29 300	1.27
4[c)]	P(Br^i BuEMA$_9$-*co*-MEA$_{23}$)-*g*-PMEA	520:1:1.6:1.6[e)]	DMF/Anisole	90	30	131 300	181 700	1.38
5[c)]	P(Br^i BuEMA$_8$-*co*-HEMA$_{37}$)-*g*-PMEA	500:1:1.6:1.3[e)]	DMF/Anisole	90	30	120 300	140 400	1.17

[a)]The composition and subsequently the number average molecular weight of the linear precursors have been determined by ^{1}H NMR experiments; [b)]Estimated by SEC employing the PS calibration curve; [c)]Obtained by SEC employing the light scattering detector; [d)]$[M]_0:[I]_0:[CTA]_0$;[e)]$[M]_0:[I]_0:[CuBr]_0:[PMDETA]_0$.

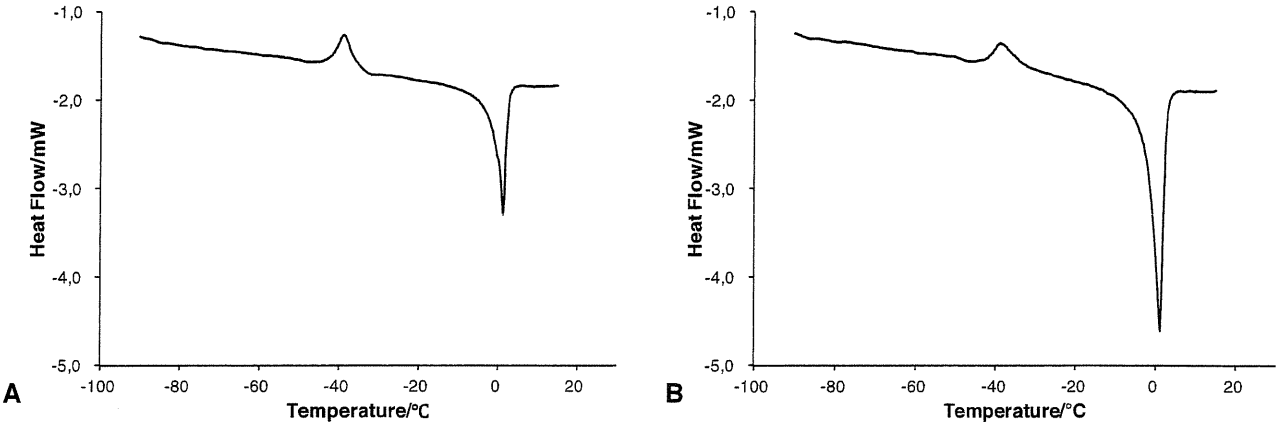

Figure 2. DSC heating curves of the graft copolymer–water systems: (A) graft copolymer **4** with the water content of 9.9 wt%; (B) graft copolymer **5** with the water content of 16.3 wt%. Heating rate is 5.0 °C min^{-1}.

phenomenon attributed to the phase transition of ice from amorphous to crystalline.[1d] The water capable of such a transition is defined as the freezing bound (intermediate) water. Besides the freezing bound water, the water restrained by a hydrated polymer includes two other types of water—free and nonfreezing water. Thus, the water content (WC) at equilibrium WC (wt%) = W_{Nf} (wt%) + W_{Fb} (wt%) + W_F (wt%), where W_{Nf}, W_{Fb}, and W_F are the contents of the nonfreezing water, freezing bound water, and free water, respectively. The platelet compatibility of the polymeric material is ascribed to the existence and is proportional to the amount of the freezing bound water.[1] When in contact with blood, the polymer surface absorbs water which forms a specific structure on the surface. The layers of different water structures follow in this order: polymer surface → nonfreezing water → freezing bound water (intermediate water) → free water → bulk water. When the freezing bound water layer has sufficient thickness, it prevents the biocomponents (cells and/or proteins) from contacting directly the polymer surface or nonfreezing water on the polymer surface.

The structure of water in the graft copolymers was investigated by DSC. The thermograms in the heating process are shown in Figure 2. A characteristic exothermic peak was found for the polymers at around –40 °C: the peak is due to the cold crystallization of water in the hydrated polymer, and serves as the evidence of existence of the freezing bound water in both graft copolymers. The endothermic peaks observed on the thermograms are ascribed to the melting of the ice originating from both free water and freezing bound water.[1] By taking into account that the heat of fusion of the ice derived from the bulk water is 334 J g^{-1},[1] and making the assumptions that $W_{Fb} \propto \Delta H_{cc}$, and $(W_{Fb} + W_F) \propto \Delta H_m$, where ΔH_{cc} and ΔH_m are the enthalpy of cold crystallization and the fusion enthalpy of ice, respectively,[1] the amounts of all three kinds of water are quantified (Table 2). Hence, the graft copolymer **4** contains more freezing bound water than the graft copolymer **5** which comprises the PHEMA backbone. Furthermore, if compared with the linear PMEA of the molecular weight of $\overline{M}_w$ = 78 000 Da, at approximately same equilibrium WC the graft copolymer **4** contains about 2.5 times less amount of the freezing bound water.[1a]

Further elucidation of the blood compatibility of these graft copolymers by platelet adhesion tests is necessary to conclude whether these materials are suited for applications in medical devices.

4. Conclusion

In conclusion, we have successfully built complex macromolecular architectures such as graft copolymers incorporating PMEA grafts which may have potential as blood compatible materials. Merging the robust and versatile CRP techniques, such as RAFT and ATRP, allows excellent control over the size and topology of the macromolecules, and

Table 2. Water content of the graft copolymers.

Entry	Graft copolymers	ΔH_{cc} [J g^{-1}]	ΔH_m [J g^{-1}]	WC [wt%]	W_{Nf} [wt%]	W_{Fb} [wt%]	W_F [wt%]
4	P(Br^i $BuEMA_9$-*co*-MEA_{23})-*g*-PMEA	6.7	16.5	9.9	5.0	2.0	2.9
5	P(Br^i $BuEMA_8$-*co*-$HEMA_{37}$)-*g*-PMEA	4.4	33.3	16.3	5.0	1.3	10.0

Macromolecular Journals
Macromol. Rapid Commun. **2012**, DOI: 10.1002/marc.201100698

provides effectual tool for integration of distinct functional monomers into advanced polymeric structures. Scrupulous thermal analyses of the products unambiguously points toward the existence of the freezing bound water which, in turn, is one of the key factors responsible for the blood compatibility.

Supporting Information

Supporting Information is available from the Wiley Online Library or from the author.

Acknowledgements: Project 10-082707 funded by the Danish Agency for Science, Technology and Innovation is acknowledged for financial support.

Received: October 24, 2011; Revised: November 24, 2011; Published online: ; DOI: 10.1002/marc.201100698

[1] a) M. Tanaka, A. Mochizuki, N. Ishii, T. Motomura, T. Hatakeyama, *Biomacromolecules* **2002**, *3*, 36; b) E. Hirota, K. Ute, M. Uehara, T. Kitayama, M. Tanaka, A. Mochizuki, *J. Biomed. Mater. Res.* **2006**, *76A*, 540; c) M. Tanaka, A. Mochizuki, *J. Biomater. Sci.* **2010**, *21*, 1849; d) M. Tanaka, A. Mochizuki, *J. Biomed. Mater. Res.* **2004**, *68A*, 684.

[2] N. Saito, S. Motoyama, J. Sawamoto, *Artif. Organs* **2000**, *24*, 547.

[3] a) W. A. Braunecker, K. Matyjaszewski, *Prog. Polym. Sci.* **2007**, *32*, 93; b) K. Matyjaszewski, N. V. Tsarevsky, *Nat. Chem.* **2009**, *1*, 276.

[4] a) G. Moad, E. Rizzardo, S. H. Thang, *Aust. J. Chem.* **2005**, *58*, 379; b) G. Moad, E. Rizzardo, S. H. Thang, *Aust. J. Chem.* **2009**, *62*, 1402; c) L. Barner, T. P. Davis, M. H. Stenzel, C. Barner-Kowollik, *Macromol. Rapid Commun.* **2007**, *28*, 539.

[5] A. S. Brar, T. Saini, *Polym. J.* **2006**, *38*, 1023.

[6] a) M. Bednarek, K. Jankova, S. Hvilsted, *J. Polym. Sci., Part A: Polym. Chem.* **2007**, *45*, 333; b) N. M. L. Hansen, D. M. Haddleton, S. Hvilsted, *J. Polym. Sci., Part A: Polym. Chem.* **2007**, *45*, 5770.

[7] J. F. J. Coelho, J. Gois, A. C. Fonseca, R. A. Carvalho, A. V. Popov, V. Percec, M. H. Gil, *J. Polym. Sci., Part A: Polym. Chem.* **2009**, *47*, 4454.

[8] a) W. Steinhauer, R. Hoogenboom, H. Keul, M. Moeller, *Macromolecules* **2010**, *43*, 7041; b) R. Hoogenboom, A.-M. Zorn, H. Keul, C. Barner-Kowollik, M. Moeller, *Polym. Chem.* **2012**, DOI: 10.1039/c1py00344e.

[9] G. Liu, Q. Qiu, W. Shen, Z. An, *Macromolecules* **2011**, *44*, 5237.

[10] K. L. Beers, S. G. Gaynor, K. Matyjaszewski, S. S. Sheiko, M. Möller, *Macromolecules* **1998**, *31*, 9413.

[11] L.-S. Wan, H. Lei, Y. Ding, L. Fu, J. Li, Z.-K. Xu, *J. Polym. Sci., Part A: Polym. Chem.* **2009**, *47*, 92.

[12] R. Venkatesh, L. Yajjou, C. E. Koning, B. Klumperman, *Macromol. Chem. Phys.* **2004**, *205*, 2161.

[13] a) M. Seo, S. Shin, S. Ku, S. Jin, J.-B. Kim, M. Ree, S. Y. Kim, *J. Mater. Chem.* **2010**, *20*, 94; b) Y. Zhang, Z. Shen, D. Yang, C. Feng, J. Hu, G. Lu, X. Huang, *Macromolecules* **2010**, *43*, 117; c) Y. Li, Y. Zhang, D. Yang, J. Hu, G. Lu, X. Huang, *J. Polym. Sci., Part A: Polym. Chem.* **2010**, *48*, 2084; d) Y. Zhang, Y. Li, Y. Li, D. Yang, J. Hu, G. Lu, X. Huang, *J. Polym. Sci., Part A: Polym. Chem.* **2010**, *48*, 2622; e) Y. Li, Y. Zhang, D. Yang, Y. Li, J. Hu, C. Feng, S. Zhai, G. Lu, X. Huang, *Macromolecules* **2010**, *43*, 262; f) X. Song, Y. Zhang, D. Yang, L. Yuan, J. Hu, G. Lu, X. Huang, *J. Polym. Sci., Part A: Polym. Chem.* **2011**, *49*, 3328; g) C. Feng, Y. Li, D. Yang, J. Hu, X. Zhang, X. Huang, *Chem. Soc. Rev.* **2011**, *40*, 1282.